Model of particle growth in silane discharges

Alan Gallagher*
JILA, University of Colorado and National Institute of Standards and Technology, Boulder, Colorado 80309-0440
(Received 8 October 1999; revised manuscript received 8 February 2000)

The growth of silicon particles in the neutral plasma region of pure silane, rf capacitively coupled, steady-state discharges is calculated with a homogeneous, plasma-chemistry model. Plasma conditions are typical of those used in hydrogenated amorphous silicon (a-Si:H) device production. SiH_3 and SiH_3^- grow into particles by the step-by-step addition of silicon atoms, primarily due to reactions with SiH_3. Attrition of growing $Si_xH_m^z$ radicals and ions with z charges, which are ''particles'' for large x, occurs by diffusion of neutral and positively charged radicals to the electrodes. Rate coefficients for electron, ion, radical, and silane collisions with the $Si_xH_m^z$ for $x=1-10^5$ are estimated from detailed considerations of the literature and relevant physics. Self-consistent anion, cation (n_+), and electron (n_e) densities and charge fluxes are used, and charge neutrality is maintained. Typically $n_+/n_e \cong 100$, which causes a large fraction of neutral particles and thereby a major particle flux into the growing a-Si:H film. The density of visible particles ($x>10^4$) varies many orders of magnitude with relatively minor changes in discharge power, pressure, and electrode gap. This parameter dependence agrees with experiment, and by adjusting collision parameters within a reasonable range the calculated particle densities can be brought into exact agreement with experiment. An additional result of the model, which has not yet been detected, is that Si_xH_m clusters with $3<x<30$ are continuously deposited into growing films, and for typical conditions yield a very significant fraction (1–10 %) of total film growth.

PACS number(s): 52.80.−s, 52.65.−y

I. INTRODUCTION

Hydrogenated amorphous silicon (a-Si:H) photovoltaics (PV) or thin-film transistors are most frequently grown from dc of rf plasmas in pure silane (SiH_4) or SiH_4 diluted into H_2. Silicon particles also grow in these plasmas as an unintended side effect, and some of these are incorporated into devices. This has stimulated a desire to understand the causes and behavior of these particles, and if possible to control particle incorporation into growing films.

Many particle-in-plasma measurements have been carried out in noble gas discharges, where the cation density (n_+) equals the electron density (n_e). Due to the higher electron velocity, this causes most of the particles to be negatively charged and suspended in the plasma by electrostatic forces [1]. However, this expectation of efficient particle trapping appears to be misleading for silane discharges, as a large flux of 2–8-nm radius (r_p) particles have been observed to continuously deposit into a-Si:H films from rf silane discharges [2]. Thus, a significant fraction of this size particle must become neutral and escape the plasma. The present model explains why this occurs; in an attaching gas like silane $n_+ \gg n_e$ and this causes a large fraction of particles to be neutral. The model presented here also explains measured trends in particle growth and density from a recent experiment that utilized typical device deposition conditions [3]. However, several other experiments in silane or silane–noble-gas mixtures have reported different results, in particular particle agglomeration. This only occurs for relatively high plasma charge densities and accompanying large densities of small particles. The present calculation applies to conditions where small-particle densities are much smaller and their agglomeration is not significant. The latter conditions are more representative of those used for the production of a-Si:H devices.

The question of what role these incorporated Si particles play in the electronic properties of a-Si:H devices is not known, and probably varies with plasma conditions and device. It is well known that higher powers or film-growth rates cause film electronic quality to deteriorate, and as will be shown below particle incorporation increases very rapidly with power. However, there are other factors, such as cation bombardment and increased heavy-radical contributions to film growth, that also increase with power, and all of these are only *correlations*. Ellipsometry observations have shown that particle incorporation can influence the film optical properties, [4] but this does not prove that electronic quality under device-production conditions is affected. The particles are made of the same material (Si and H) as the film, but they may have a different structure due to the different growth environment in the plasma. (It seems likely that the isolated nanocrystals that are sometimes observed in a-Si:H films were formed in the plasma.) One would expect most problems to occur at the interfaces between particles or clusters and the remaining film, particularly underneath the particles since the particle and film have different shapes at contact, and this region is shadowed from the plasma and incident radicals. However, hydrogen might passivate many of these sites, and until device or film-quality measurements are made while changing only particle incorporation, the net influence of particle incorporation remains uncertain. Also, in cases where microcrystalline films are desired, such as some doped layers of PV cells, one may wish to assist incorporation of crystalline particles. In either event, finding ways to control particle incorporation into a-Si:H films is desirable, and a primary motivation of this study. This is the first attempt to develop a detailed plasma and chemistry model to under-

*Also at Quantum Physics Division, NIST.

stand particle growth and release into *a*-Si:H films.

Since the initial observation of particles in silane discharges by Roth *et al.* [5], and in silicon processing discharges by Selwyn [6], a variety of measurements and models have shown that particles negatively charge and are thereby trapped in the neutral plasma of a rf discharge [7]. There they grow until of sufficient size to be dragged away to pumps by gas flow, perhaps aided by local plasma modification at plasma edges where they accumulate [6,8]. These plasma models have not considered particle losses to the electrodes or the specific conditions of discharges used to produce *a*-Si:H devices. Thus, it came as a surprise that visible particles can be continuously deposited into *a*-Si:H films [2].

It has also become apparent that the appearance of visible particles suspended in the plasma depends strongly on plasma parameters, often with an abrupt transition as power or pressure increases [9]. Choi and Kushner have provided a qualitative understanding of the cause of this sensitivity to power and pressure [10]. They note that, in essence, particle growth competes with diffusive loss and the competition depends on these parameters. Of course, such diffusive loss requires that the particle first become neutralized, so a full model must consider the particle charge distribution that results from electron and cation collisions with the particles. This particle charge distribution will be a function of particle size and the n_+/n_e ratio, so a viable model must obtain this ratio versus discharge parameters in the presence of particles. This is done here, where the ratio is combined with a collisional and chemical model for growth from SiH_3 and SiH_3^- into Si_xH_m and $Si_xH_m^-$ clusters and then into (mostly silicon) particles.

The present calculation depends on a large number of electron, ion, and particle collisional rate coefficients, all required versus x and z for $Si_xH_m^z$ particles of charge zq, for many orders of magnitude of x. To obtain these a recent review by Perrin has been heavily utilized and was very valuable in obtaining what we believe are reasonable values [11]. (Neither the review nor the present model would be very realistic without the many studies on which that review is based, but these are too numerous to credit here.) However, these primarily involve $x<10$ and it has been necessary to go far beyond the data and theories reviewed there. Thus, a major portion of this manuscript is devoted to discussions of the basis of the assumed rate coefficients. Tests are reported for the sensitivity of the results of changes in some of the least certain values.

II. DETAILS OF THE CALCULATION

A. Discharge conditions

The primary emphasis is on parallel-plate, capacitively-coupled, rf or high-frequency discharges, for powers and pressures commonly used for the deposition of *a*-Si:H devices. [Typically, silane density is $(10^{15}-10^{16})/cm^3$, the electrode gap is 1–10 cm, and the film-growth rate is 0.1–1 nm/s]. The calculation also applies, with some modification, to the negative-glow region of a dc discharge. Only pure silane discharges will be treated here; the methods described can be extended to the silane/H_2 mixtures that are also commonly used. A neutral plasma typically fills the central 50–80 % of the electrode gap, and particles grow and reside primarily within this region. The sheath between the neutral plasma and electrodes contains a high electric field that excludes negatively charged particles and rapidly drifts cations to the electrodes.

Particle growth in the neutral plasma *will be treated with a homogeneous model*, using average electron, ion, and radical densities and temperatures appropriate to this neutral plasma region. In this model negatively charged particles (anions) are trapped in the discharge, neutral particles can diffuse to the electrodes, and positively charged particles (cations) that diffuse into the sheaths drift to the electrodes. This particle loss competes with growth, so that particle densities are a monotonically decreasing function of particle size.

In normal deposition discharges, gas flow drifts particles larger than several nm to the downstream end of the discharge, where they grow to μm size and are eventually dragged away to the pumps. The use here of a homogeneous model for initial particle growth is reasonable for these discharges, because the spatial distribution of greater than 1 nm size particles within the quasineutral plasma region does not greatly effect particle growth and losses. However, it is important to recognize that when effects such as gas flow, ion wind, and thermophoresis concentrate particles within smaller regions, this will alter the local particle charge balance and increase the escape rate, causing fewer particles to grow to visible sizes compared to the present calculation.

B. Overview of the model

Particles grow primarily from SiH_3^- anions and SiH_m radicals, first into $Si_xH_m^-$ ions and Si_xH_m radicals, then with increasing x into clusters containing multiply bonded silicon, and finally into compact, primarily silicon material with a largely H-terminated surface, equivalent to the *a*-Si:H material that grows on the electrodes. (Crystalized particles are also possible, and even likely with H_2 dilution.) We will use the word ''particle'' to describe all $x>1$, $Si_xH_m^z$ radicals, clusters, ions, and clumps of *a*-Si:H, regardless of size, structure, or charge equal to zq, where q is the proton charge. We will use $n(x,z)$ to denote the density of $Si_xH_m^z$, *ignoring the* H *content of particles and reactants in all parts of the calculation*.

The calculation is carried out by first establishing the densities of the $x=1$ particles, and then iteratively calculating heavier particle densities from collisions and diffusion of higher particles. *A key assumption used is that no collision decreases the number of* Si *atoms in a particle*. As a result, starting with densities $n(1,z)$ for $z=-1,0,-1$, the $n(2,z)$ with $z=1,0,-1$ can be calculated. Then the $n(3,z)$ are calculated using these $n(1,z)$ and $n(2,z)$, and this $x\rightarrow x+1$ iteration is repeated to $x=60$, where $z=-2$ is also stable. Similar $x\rightarrow x+1$ iterations are then carried out with $z=1,0,-1,-2$ until $z=-3$ is stable at $x=210$, etc. to $x=10^4$ (particle radius $r_p=3.6$ nm,) or 10^5 ($r_p=7.8$ nm) corresponding to measured particle sizes.

For each $x\rightarrow x+1$ step the rate of neutral-particle diffusive loss competes with the growth rate. Thus, a fractional attrition of particles occurs for each growth step, and as greater than 10^4 growth steps are required to produce the

$r_p > 4$ nm particles measured in Ref. [3], the measured particle density is a very rapid function of this fractional attrition per step. Small neutral particles diffuse to the electrodes much faster than they recharge negatively, so they are largely lost from the discharge. As particles increase in size the electron-charging rate increases and the diffusion rate decreases, so that neutral-particle losses per growth step are much less severe. However, many growth steps are needed to reach $x = 10^4$, so the predicted density of visible particles is very sensitive to losses at all x values. (Only calculations to $x = 10^4$ are presented here, as the density expected for larger x is apparent from this and these calculations were done with a PC, for which iterating to $x = 10^5$ required 30 min.) In contrast to this extreme sensitivity of particle density, the radius growth rate of observable particles varies slowly with plasma parameters, and often bears a direct relation to SiH_3 density [3].

Radical densities (n_r) greatly exceed total cation (n_+) and anion (n_-) densities, so radical collisions normally dominate particle growth. The exception is the growth of $x < 100$ anions and $x < 6$ cations, which grow primarily from SiH_4 collisions. At low film-growth rate (G), pressure (P), and electrode gap (L) SiH_3 is the only significant radical, so both radical and SiH_4 growth mechanisms add one Si atom at a time to the growing particles. (Similarly, SiH_3 dominates film growth.) However, as G, P, and L increase, higher radicals (Si_xH_n with $x > 1$) add significantly to both particle and film growth. The general case is treated here by calculating the mixture of light Si_xH_m radicals with $x = 1 - 30$, and using all of their collisions with particles and film to calculate both growth rates. It is assumed that when Si_xH_m radicals with $x > 1$ incorporate into the film or the particles they add x Si atoms. This appears likely because Si-Si bonds are strong and should remain intact when one Si of the radical attaches to a Si at the film or particle surface. Since we have no direct knowledge of the probability of Si_xH_m ($x > 1$) incorporation into either particles or film, it is assumed that this is the same for both and independent of x. This is done primarily to simplify the calculation, but it appears reasonable within a commonly used model where radical attachment occurs at surface dangling bonds. Some effects of these assumptions on the results will be discussed below.

The calculation includes particle-particle collisions involving all neutral particles with $x < 30$, all positive particles with $x < 100$ and all negative particle with $x < 200$. Particle-particle collisions where both x values are greater than 200 are found to make a negligible contribution to particle growth for the plasma conditions normally chosen here. However, for conditions that yield a total $x > 200$ particle density near the total ion density this ''particle agglomeration'' does begin to appear. This sets the validity limit of the present calculation.

Only steady-state particle densities are calculated in this paper. As described above, this is done by iteratively obtaining the $n(x,z)$ densities from the $n(x' < x, z')$ densities, starting with the $x = 1 \rightarrow 2$ step. Thus, valid densities of the $x = 1$ particles with $z = 1$, 0, and -1 are required, and as particle densities are very sensitive to charging rates it is also essential to utilize reasonable values of n_e and n_+. Self-consistent values have been obtained for these crucial densities as follows. The discharge is described by values for P, L, and G_1, the film-growth rate due to SiH_3 incorporation. Then the SiH_3 density, $n(1,0)$, that is required in the neutral plasma to yield this G_1 is calculated from diffusion theory and published Si incorporation-efficiency measurements. (The SiH_3 density exceeds that of other SiH_n radicals typically by a factor of 100, because they react rapidly with SiH_4 [12,13]. This is the same reason that most film deposition is by SiH_3.) Next, from radical diffusion theory and published rf-plasma models for the efficiency of electron collisional dissociation of silane, n_e is obtained from G_1. The values of $n(1,1)$ and $n(1,-1)$ are then obtained using n_e, rate coefficients for their formation by electron collision and rates for their destruction, which is primarily due to collision with SiH_4. Finally, the n_+ and n_- values are obtained from the full calculation by requiring charge neutrality in this neutral-plasma region. This results when the cation density is sufficient to neutralize anions at the rate they are produced, since anions cannot escape the plasma. As described in Sec. II C, an adjustable parameter related to cation diffusive loss is also used to obtain exact charge neutrality. The quantitative relations used to obtain the n_e, $n(1,1)$, $n(1,0)$, and $n(1,-1)$ values as functions of the discharge parameters P, L, and G_1 are derived in Appendix A.

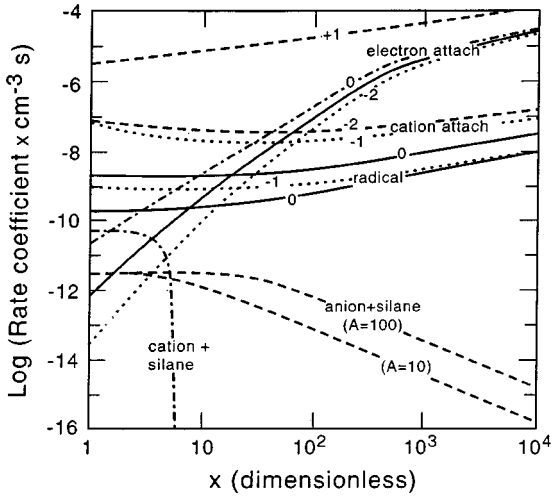

FIG. 1. Rate coefficients for electron attachment, $y = 6$ cation attachment, and $y = 1$ radical attachment to a particle containing x Si atoms. The particle charge z is indicated by the number by near each line, and y is the number of Si atoms in the cation or radical.

Equally important to the validity of the results are reasonable rate coefficients for binary collisions between pairs of the species: electron, cation, anion, silane, radical, and particles of all charge and size. The quantitative basis for the values used in the calculation is provided in Appendix B. The resulting rate coefficients and typical rates are given in Figs. 1 and 2.

The probability that a particle of size x will escape as a neutral or cation depends on the fraction in those charge states, as opposed to anions that are trapped in the plasma. This, in turn, depends on the number of negative charges that can reside on a particle, so it is important to establish at what x values multiple charging can occur. It is common in the aerosol field, where this issue is most studied, to recognize two major constraints on multiple charging of particles [14].

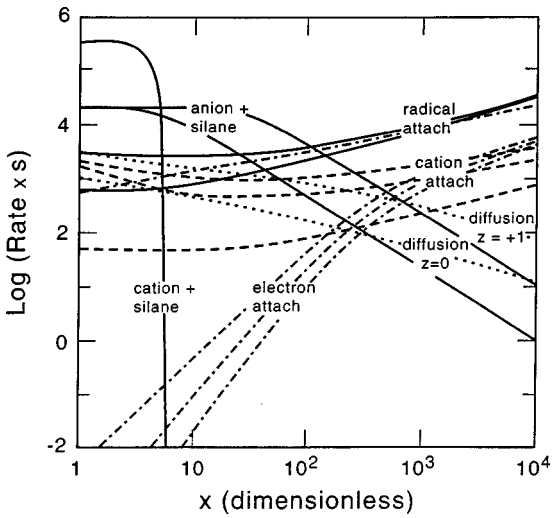

FIG. 2. Rates for electron attachment, $y=6$ cation attachment, and $y=1$ radical attachment to a Si_xH_m particle of charge z for n_S, n_e, and n_+ conditions of Fig. 5(b), as given in Table I. Charged-particle reactions with silane, and diffusion rates of neutral and positive particles are also shown for these conditions.

The first results from the tunneling of one electron through the potential barrier outside the particle, as shown in Fig. 3 for a particle of radius $R_p=0.4$ nm. The second (Rayleigh) limit reflects the ability of water particles to remain intact using surface tension forces to counteract the charge repulsion. Silicon atoms are bound together by much larger forces ($\sim$5 eV per atom), so only the first constraint applies to the silicon particles of interest here. This is evaluated in Appendix C to obtain the x values where $z=-2$, -3, etc. become stable, and this result is used in the calculation to set the size threshold for each charge state.

C. Particle-density equations

When x exceeds perhaps 50, the $Si_xH_m{}^z$ ''molecule'' is expected to consist of a roughly spherical structure of cross-linked Si atoms with an occasional H within and a primarily H-terminated surface, equivalent to the a-Si:H film. This structure is generally thought of as a particle and the smaller x values as molecular negative ions or radicals, but for continuity we describe all as a ''particle.'' Although m is ignored in the calculation, it must actually be a value that prevents the neutral particles from reacting with silane but allows them to react with the film. Thus, they behave as ''monoradicals'' like SiH_3 that have a single dangling bond. With the exception of the $x<200$ anions and $x<6$ cations, the charged particles also do not react with stable gases. Large x particles have a largely H-passivated surface, but just as for the film we expect an occasional dangling Si bond. These particles will stick to the film surface due to van der Waals forces, and eventually incorporate by Si-Si bonding.

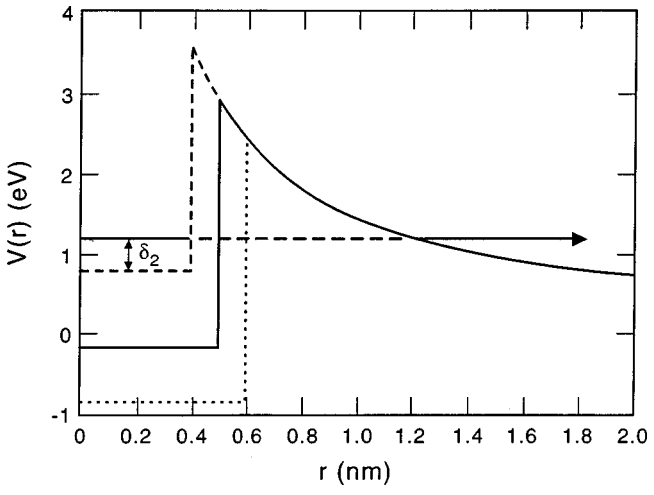

FIG. 3. Potential $V(r)$ felt by one electron versus radius (r) from the center of a Si particle charged by a second electron. $V(r)$ is shown for three different particle radii R_p, with a step equal to the electron affinity (EA) occurring at R_p. Tunneling through the potential barrier is shown for the smallest particle. If $V(r)$ plus the interelectron Coulomb repulsion energy (δ_2) is below 0, both electrons can be attached to the particle.

Most of the anion and cation densities are on $x<200$ particles and most of the radical density has $x<10$. Thus, collisions of these lighter species (labeled with No. Si$=y$) and electrons with other particles (No. Si$=x$) dominate particle charging and growth.

For the growth of $x>200$ particles, the calculation has already produced the densities, $n(y,z')$, of the lighter particles that dominate collision rates, and these are distinguishable from the particles undergoing an $x\rightarrow x+1$ growth step. Thus, a net collision rate $R(x,z)_J=\Sigma k(x,z,y,z')_J n(y,z')$, summed over y and z', can be defined for each reaction J. However, a simplification that speeds the calculation without significant loss of accuracy for $x>200$ is to lump all y radical contributions to particle growth into an equivalent rate for adding only one Si atom during an $x\rightarrow x+1$ step. For the $z=0$ case this is done by using an effective rate $R(x,z)_{R\,\mathrm{eff}}=F(x,z)R(x,z)_{R1}$, where $R(x,z)_{R1}=k(x,z,1,0)_{\mathrm{RR}}n(1,0)$ is the rate due to SiH_3 only. The multiplier $F(x,z)$ is given by $\Sigma_{y=1}^{30}k(x,z,y,0)_{\mathrm{RR}}yn(y,0)/k(x,z,1,0)_{\mathrm{RR}}n(1,0)$; it normally ranges from 1–5 and is nearly independent of x for $x>200$. Thus, the calculation generally uses $F(x,z)=F(z)$ independent of x, which minimally alters the results as long as the same factor is used below in both $S(x)_z$ and $M(x)_{z,z}$. As will be described below, a similar simplifying assumption is used for particle growth due to cations.

From Fig. 4, which applies for $x>200$ where the light radicals are distinguishable from the $n(x,z)$ under consideration, the $n(x,z)$ can be obtained from the $n(x-1,z')$ densities with a matrix equation of the form $dn(x,z)/dt=S(x)_z-M(x)_{z,z'}n(x,z')$. This expresses the fact that each population $n(x,z)$ arises from a source term $S(x)_z$ due to transfer from all particles with fewer Si atoms, plus some terms $M(x)_{z,z'}n(x,z')$ that represent mixing between adjacent z values with the same x. The loss of $n(x,z)$ due to transfer to $x+1$ and diffusion is contained in the diagonal term $M(x)_{z,z}n(x,z)$. Note that, since only electron, $z=1$ cation, $z=-1$ anion, and neutral-radical collisions are included, $M(x)_{z,z'}$ has only diagonal and first off-diagonal nonzero terms. For the steady-state case of $dn(x,z)/dt=0$ this yields

$$S(x)_z=M(x)_{z,z+1}n(x,z+1)+M(x)_{z,z-1}n(x,z-1)+M(x)_{z,z}n(x,z), \quad (1)$$

where

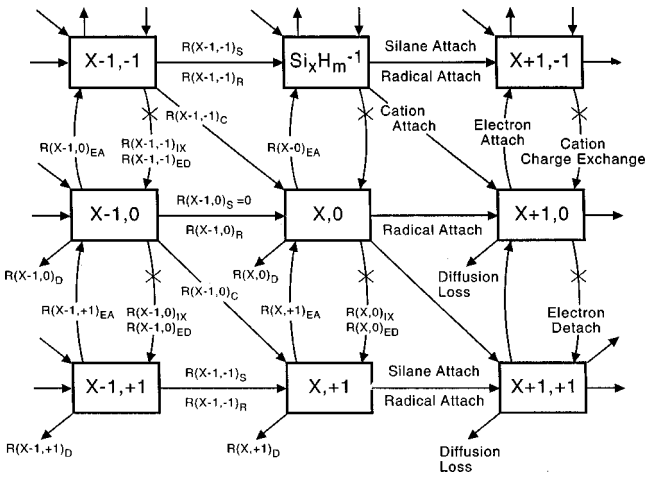

FIG. 4. Diagram of the collision processes that cause particle growth, charging, and diffusive loss for $x>210$ particles. Particles $Si_xH_m^z$ are shown in boxes labeled x,z and collisional transfer between these is represented by arrows. The collisional rates are written as $R(x,z)_j$ where j describes the process, and x,z refer to the initial particle. For the attachment of Si from a radical $j=R$, from a cation $j=C$, from silane $j=S$. Anion attachment plays a very minor role in growth and charging, so it is not shown or included in the calculation. For electron attachment j is EA, for electron detachment j is ED, and for cation charge exchange without attachment j is IX. Diffusive loss is labeled $j=D$. Cation and radical attachment are shown as adding a single Si, whereas both add a range of Si atoms. In the calculation the cation attachment adds six Si and the radical attachment adds one Si at a rate that represents a sum over all radical sizes.

$$S(x)_z=[R(x-1,z)_{R\,\mathrm{eff}}+R(x-1,z)_S]n(x-1,z)+R(x-1,z-1)_{\mathrm{IA}}n(x-1,z-1),$$

$$M(x)_{z,z-1}=-R(x,z-1)_{\mathrm{TX}}-R(x,z-1)_{\mathrm{ED}},$$

$$M(x)_{z,z+1}=-R(x,z+1)_{\mathrm{EA}},$$

$$M(x)_{z,z}=R(x,z)_{\mathrm{ED}}+R(x,z)_{\mathrm{IX}}+R(x,z)_{IA}+R(x,z)_S+R(x,z)_{R\,\mathrm{eff}}+R(x,z)_{\mathrm{EA}}+\delta_{z,0}R(x,0)_D+\delta_{z,1}R(x,+1)_D.$$

The rates $R(x',z')_J$ refer to a collision that transforms the x',z' particle into an x,z particle by process J, or to diffusive loss. With reference to Fig. 4, $J=S$ (or R) is a collision with silane (or a radical), $J=\mathrm{IA}$ is positive ion attachment, $J=\mathrm{IX}$ is ion charge exchange, $J=\mathrm{ED}$ is electron-induced detachment, $J=\mathrm{EA}$ is electron attachment, and $\delta_{z,0}R(x,0)_D$ and $\delta_{z,1}R(x,+1)_D$ terms are neutral and positive particle diffusion to the electrodes, where $\delta_{z,z'}$ is the delta function.

In Eq. (1), $M(x)_{z,z}$ is the relaxation rate for each density $n(x)_z$ to come to steady state with the density of particles with one less Si atom. For typical discharge conditions the corresponding time is much less than 1 ms. However, it is important to recognize that *the total time after discharge initiation in which the density $n(x,z)$ reaches steady state is the sum of all $1<x'<x$ decay rates*. In essence, each density x is delayed relative to the $x-1$ density by a time $[M(x)_{\langle z,z\rangle}]^{-1}$, where $\langle z,z\rangle$ refers to a density-weighted average over z. Since x can be a very large number, this total delay can be quite significant compared to 1 s. However, transients will not be described in this paper.

The solution of the (z,z' matrix) equation $M(x)n(x)=S(x)$ is $n(x)=M(x)^{-1}S(x)$, and in principle one can use this to iteratively solve for each set of $n(x,z)$ using the previous set of $n(x-1,z')$. However, it is shown in Appendix B that the rates $R(x,z-1)_{\mathrm{IX}}$ and $R(x,z-1)_{\mathrm{ED}}$ can be deleted without loss of accuracy, and this removes the $M(x)_{z,z-1}$ term in Eq. (1). It is then more direct to carry out the $n(x,z')\rightarrow n(x+1,z)$ iteration by consecutively decreasing z from $+1$ to 0 to -1, and so forth. This avoids the matrix inversion and is faster.

As x increases the average negative charge on the particles increases, but for $x<10^4$ or $r_p=3.6$ nm the average z is less than 3. Thus, only z values to ~ 6 are required to establish densities of visible particles, and for much of the $x=1-10^4$ range a smaller z range is required. Obtaining the iterative solutions of Eq. (1) to $x=10^4$ thus requires only a few minutes on a PC.

It is also possible to modify the iterative solution to an integration for $x>10^3$ by separating the calculation of charge ratios at each x from the calculation of growth and attrition. This is outlined in Appendix D to show how the calculations can be extended efficiently and accurately to larger-x values. This method was used to provide confidence in the accuracy of the large-x iterative solutions, but only iterative results for $x=1-10^4$ are presented here.

The iterative solutions of the particle-growth equations for $x<200$ are different, since the particle with x Si atoms and the radical or ion with y Si atoms are frequently indistinguishable. Furthermore, the reactions of an x Si-atom particle with $y>x$ particles is significant, yet the $n(y,z')$ have not been determined when the $n(x,z)$ must be established. This situation, and the method of solution, is treated in detail in Appendix E.

The film-growth rate G is dominated by neutral radical diffusion, and by generalization of Eq. (A1) to many radicals is given by

$$G=0.4\pi L^{-1}\rho^{-1}\sum_{y=1}^{30} n(y,0)yR(y,0)_D. \qquad (2)$$

III. RESULTS

We will primarily consider conditions similar to those of Ref. [3], as other measurements of particle growth in pure silane [15] or a silane-He mixture [16] did not observe particles by light scattering until a rapid agglomeration stage occurred. Typically $r_p\sim 5$ nm particles agglomerated, whereas at the highest-particle densities covered by this calculation agglomeration of $r_p>1$ nm particles is just beginning to be significant. It is not the purpose of this calculation to explain such high-particle densities or large-particle agglomeration, which should not occur under device-production conditions. Thus, the range of conditions reported here stops short of those that produce such large-particle densities.

Typical experimental conditions in Ref. [3] were $n_S=10^{16}$ cm^{-3}, $G=2$ Å/s, $L_D=1.5$ cm, and $T=300$ K, but a

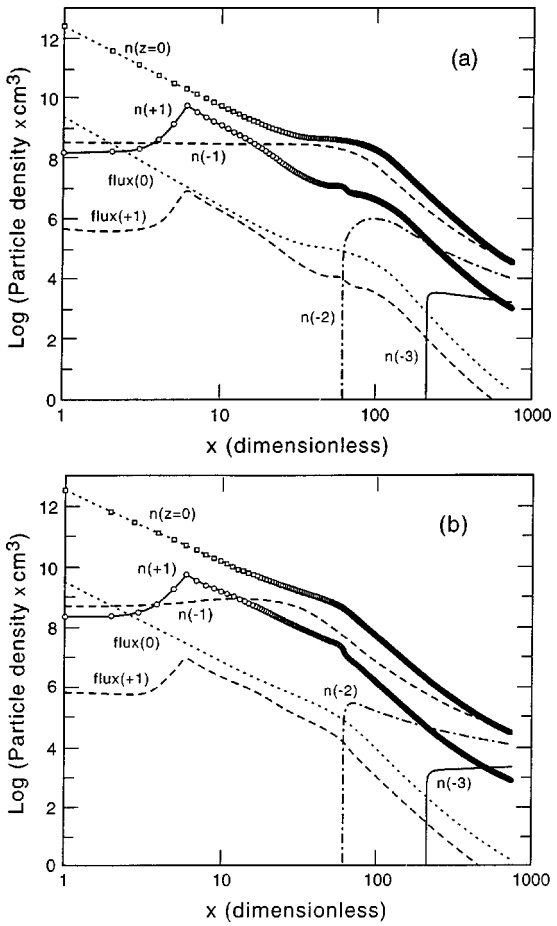

FIG. 5. Particle density $n(z)$ versus x, the number of Si atoms in the particle, and particle charge z. The diffusion flux of $z=0$ and $+1$ particles out of the neutral plasma region is also indicated, where the units are $10^6\,\mathrm{cm}^{-3}\,\mathrm{s}^{-1}$ (i.e., the flux for $x=z=0$ is $\sim 2\times 10^{18}\,\mathrm{cm}^{-3}\,\mathrm{s}^{-1}$). The plasma conditions for parts (a) and (b) are given in Table I.

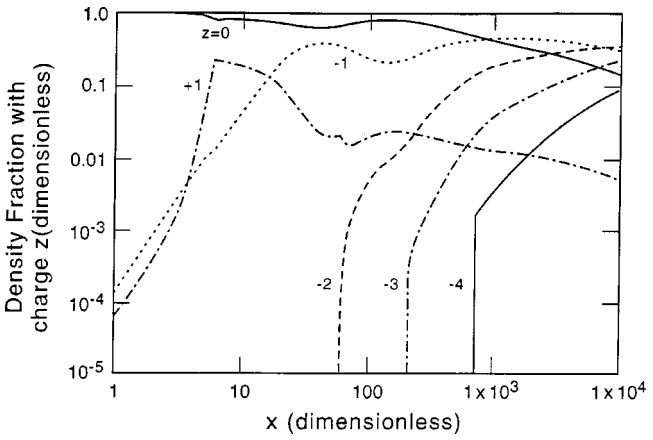

FIG. 6. Particle density $n(x)_z$ as a fraction of all particles with the same x value (the number of Si atoms in the particle), for the z values (particle charge) indicated. The plasma conditions are those of Fig. 6(a), given in Table I.

larger L and lower n_S are used in most device production and the calculation has been carried out for $L=1.4-4$ cm and $n_S=0.35-1\times 10^{16}\,\mathrm{cm}^{-3}$. The overall G range covered is from 0.5–10 Å/s, while for each L, n_S combination G has been varied to yield a range of large- (visible) particle density from a high value near the ion density to a negligibly low value. In Fig. 5(a) we show the particle densities versus x and z, calculated for values of L and n_S in the middle of this range with G chosen to provide a midrange particle density. To clarify low-x behavior $x=1-10^3$ is covered in this figure, and the neutral and cation flux to the electrodes are shown separately. The density of each charged particle $n(x,z)$ is shown as a fraction of total x particles in Fig. 6 for the same conditions as Fig. 5(a). In Fig. 5(b) the anion-silane reaction rate coefficient has been changed by lowering A of Eq. (B6) from 100 [in Fig. 5(a)] to 10. At the same time G has been increased $\sim 3x$ to yield similar particle densities at large x. Conditions are given in Table I.

In Fig. 7 the neutral and ion surface fluxes are combined and particle densities are plotted from $x=1-10^4$ ($r_p=0.16-3.6$ nm). For comparison to particle radius, a particle silicon density of $5\times 10^{22}/\mathrm{cm}^3$, or 94% of the crystal silicon density is assumed; then $x=209(r_p/\mathrm{nm}^3)$ or $r_p=0.168x^{1/3}$ nm.) Three G values that yield a large range of $x=10^4$ particle densities are presented in Figs. 7(a)–7(c); the conditions and parameters are in Table I. The total particle density, summed over charge $n(x)_{\mathrm{tot}}$ is labeled ''Total'' in Fig. 7.

The densities in Figs. 5 and 7 refer to particles of size x, so they represent dn/dx. To change dn_{tot}/dx to particle density per nm of radius, labeled ''Total/nm'' in Fig. 7, dn_{tot}/dx is multiplied by $1\ \mathrm{nm}\times dx/dr_p=17.8x^{2/3}$. Note that Total/nm is leveling off at the right side of Fig. 7(c). This occurs because particle loss is negligible for these conditions at large x, while radical-dominated growth yields a constant dR_p/dt. (The later results from $dx/dt\propto r_p^2 dr_p/dt$ and a cross section for the Si addition that is proportional to r_p^2.) Particles start to grow at all times, so a constant dr_p/dt yields a constant Total/nm in the steady state.

In Fig. 7(b) the Total/nm line is dropping slowly, but can easily be extrapolated to $x=10^5$ ($r_p=7.8$ nm), or even 10^6 ($r_p=17$ nm) by recognizing that it eventually levels out at very large x. In Fig. 7(a) an extrapolation of the Total/nm line is not as evident, but this particle density is too small to

TABLE I. Plasma conditions related to the figures cited. In all cases $L=2$ cm and $n_s=7\times 10^{15}\,\mathrm{cm}^{-3}$.

Figure	$G1$ (Å/s)	G (Å/s)	D_p	B	A	n_e (cm^{-3})	n_+ (cm^{-3})	n_4 (cm_{-3})
5(a) and 7(b)	1.40	2.00	3.5	2.8	100	1.3×10^8	2.15×10^{10}	1.85×10^6
5(b)	2.34	4.00	3.6	2.28	10	2.17×10^8	2.8×10^{10}	1.8×10^6
7(a)	0.80	0.97	3.0	3.7	100	7.4×10^8	1.58×10^{10}	1.5×10^2
7(c)	3.6	6.83	1.3	2.20	100	3.3×10^8	4.9×10^{10}	8.3×10^9

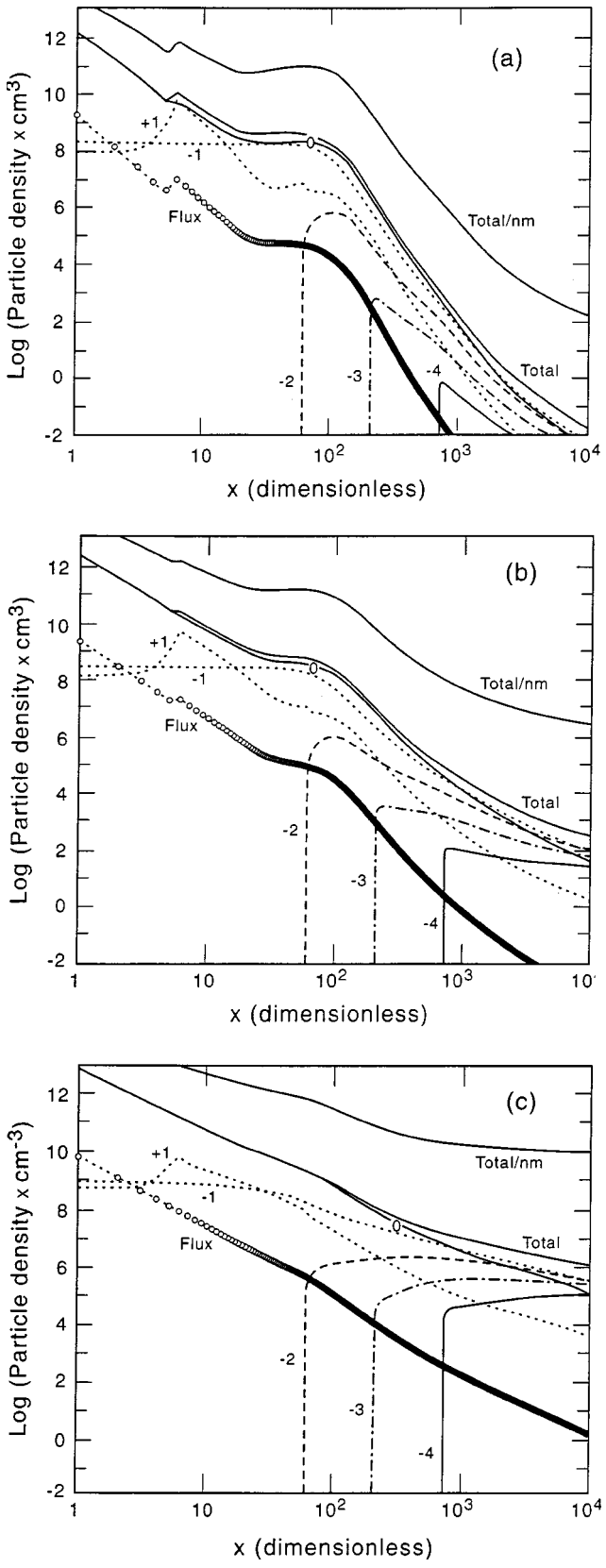

FIG. 7. Particle densities versus x, the number of Si atoms in the particle, and charge z where a number (z) is adjacent to the line. Total refers to a sum of densities over z, and Total/nm is the density per nm of particle radius. Flux refers to radical plus cation diffusive-loss flux, in units of $10^6\ \mathrm{cm}^{-3}\,\mathrm{s}^{-1}$. The plasma conditions for parts (a), (b), and (c) are given in Table I.

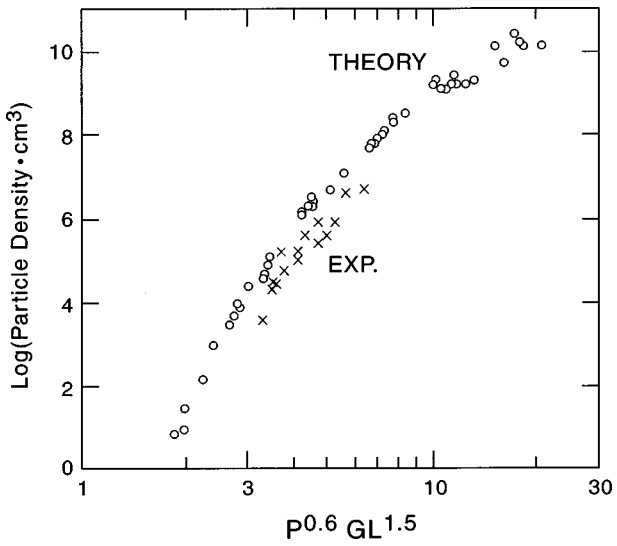

FIG. 8. Total particle density (summed over z) with $x=10^4$ (n_4) for a range of N_S and L values, where N_S is the silane density in units of $10^{16}\ \mathrm{cm}^{-3}$ and L is the effective electrode gap in cm units. (L is slightly larger than the actual gap due to a finite radical density at the boundary.) For each N_S, L combination, G has been varied to yield 4 or 5 values of n_4 that span the range of $\sim 10^1$–$10^{10}\ \mathrm{cm}^{-3}$. The abscissa is a combination of the parameters N_S, L, and G that cause all of the n_4 data to group together.

be significant. In essence, the competition between growth and loss for $x<10^4$ determines whether or not observable densities of larger particles occur.

To speed the calculations, anions with $z<-4$ have been deleted, whereas -5, -6, and -7 can occur for $x>1940$, 4300, and 8400, respectively. In Fig. 6 it can be seen by extrapolation that these higher charged ions are not very important for $x<10^4$. Their absence shifts the data in the Fig. 8 slightly to the right. At the highest reported n_4, negative charge carried by large-x particles and these neglected large $|z|$ anions become significant. It also becomes difficult to find the conditions that yield overall charge neutrality. For the entire range of parameters, which yield 10 orders of magnitude in particle density, $n_+ = 1-5\times 10^{10}\ \mathrm{cm}^{-3}$ and $n_e = 0.5-5\times 10^8\ \mathrm{cm}^{-3}$, with the larger values corresponding to higher particle densities.

In Fig. 8 the $x=10^4$ Total/nm particle density n_4 is plotted as a function of L, n_S, and G that yields a universal behavior for the full range of these parameters. (For each L and n_S several G values were used.) This universal curve is found to be a function of $n_S^{0.6}\mathrm{GL}^{1.5}$, so it is most sensitive to changes in L, next to G, and least to n_S. As can be seen by extrapolation in Fig. 7, choosing $x=10^5$ or 10^6 ($r_p=7.8$ or 17 nm) would decrease the lower-density points slightly in Fig. 8, but would not significantly change the pattern. Thus, n_4 in Fig. 8 fairly well represents the particle sizes ($r_p = 4-20$ nm) measured in Ref. [3].

The total steady-state particle density, the integral over r_p of Total/nm, is clearly not bounded for the conditions in Figs. 7(b) and 7(c). This results from ignoring, in the steady state, the time delay from discharge inception until size r_p appears. In any real discharge, particles drift, fall, or are dragged out of the neutral-plasma region by effects not in-

cluded here, before residing for the long times required to grow to large size.

To test the sensitivity of particle densities to variations in the rate coefficients, the parameter A of Eq. (B6) was lowered from 100 to 10. (As can be seen in Figs. 1 and 2, this parameter determines the x cutoff of anion growth due to silane collisions.) This greatly lowers n_4, so to clarify more subtle differences G has been raised about a factor of 3 to yield a similar n_4 value in this comparison, which is in Figs. 5(a) and 5(b) with conditions in Table I. Note that this primarily changes the $n(x,z)$ for $10<x<100$, as might be anticipated. But as can be seen in Fig. 8, a factor of 3 along the horizontal axis is a major effect, demonstrating that this anion-silane reaction is very important.

Another major uncertainty is the neutral-particle size where electron capture becomes efficient. As can be seen in Fig. 1 from the inflection in the slope of the electron-attachment rate coefficients, this occurs at $x\sim300$ for the assumed parameters. The consequence of raising this transition point to $x\sim3000$ has also been investigated, again by finding the change in G necessary to yield the same n_4 value. G must be raised a factor of 2.0 to compensate for this change in attachment probability; again this is a very large change, implying that the efficiency of electron attachment in the $10<x<1000$ region is quite important.

The calculation has also been tested for changes in the assumed anion-silane reaction rate coefficient, $k(y,1)_S$ of Appendix B. If $k(y,1)_S=0$ is used as a limiting case, this yields SiH_3^+ rather than $Si_6H_m^+$ as the dominant cation. Since the cation-particle collision rate varies as $y^{-1/2}$, this raises the rate of cation charging of particles by $\sim 2x$. This causes slightly higher neutral and positive particle fractions, and thus increased particle diffusive loss. A slightly ($\sim$20%) higher G is then required to yield the previous particle density. This is deemed a minor change in particle density from a drastic change in $k(y,1)_S$. Since cations make a minor contribution to particle growth, this is not affected.

IV. DISCUSSION

Before comparing to experiment, we will explain some features of the results. Referring to Fig. 5(a), consider first the neutral ''particles,'' which as previously noted are radicals that react with the surface but not stable gases. The lightest is SiH_3, and for $x<30$ the others result from radical-SiH_3 reactions. The density $n(x,0)$ drops rapidly with increasing x due to rapid diffusion to surfaces, until at $x\cong30$ it reaches the negative ion density $n(x,-1)$. For $x>30$ the densities $n(x,z)$ with different charges are closely coupled by cation and electron collisions. For this case of $n_+/n_e \cong200$, these rates are about equal and as a result $n(x,0) \cong n(x,-1)$ for $x>30$ (see Fig. 6). More precisely, the ratio $n(x,0)/n(x,-1)$ slowly decreases as x increases because the electron collision rate increases more rapidly (Fig. 2), since the electron-repelling surface potential decreases as x increases.

Consider next the anions in Fig. 5(a), labeled $n(-1)$, $n(-2)$, and $n(-3)$. The density $n(-1)=n(x,-1)$ is nearly constant from $x=1-50$ due to the SiH_4 growth reaction, which is much faster than cation collisional neutralization. For $x>50$, this growth reaction slows and the cation neutralizing rate gradually increases (Fig. 2), so $n(x,-1)$ as well as $n(x,0)$ decrease due to diffusive particle loss to the electrodes. Notice that as x increases to where a higher negative-charge state ($-N$) becomes stable, $n(x,-N)$ rapidly reaches a slowly changing ratio of the other $n(x,z)$ (see Fig. 6). This ratio is maintained by electron and cation charge-transfer collisions, whose rates are much greater than diffusive loss of neutral particles. Thus, the entire distribution of charge decays as a group with increasing x. The fractional decay per growth step is primarily the neutral fraction times its diffusion rate, divided by a z-weighted growth rate. (This growth rate is almost independent of z for large x.) Cation diffusive loss also contributes but is much smaller than the neutral flux since, as can be seen in Fig. 5(a), $n(x,0)/n(x,1)\gg1$.

Next consider the cations in Fig. 5(a), labeled $n(+1)$ in the figure. The anion density, $n(-1)$ is larger even though the cations are produced at a much higher rate. This occurs because the $Si_xH_n^+$-SiH_4 growth reaction is very rapid for $x=1$ (Fig. 2). However, as x increases this reaction slows and essentially terminates for $x>6$; further growth is due to collisions with the much lower density radicals. Thus, $x=4-8$ dominate $n(+1)$. (Not all of the $Si_xH_m^+ + SiH_4$ reactions for $x\leqslant7$ have been measured, so the exact position of this cation-density peak is uncertain, but its existence appears to be an inevitable consequence of the published data.) Evidence of such a cation peak has appeared recently [17], but is not consistent with measurements of cations that impinge on the substrate during the discharge. The probable cause of this is discussed in more detail in Ref. [18]. For $x>50$, $n(+1)$ also reaches a slowly changing ratio to the other $n(z)$, as seen in Fig. 6, since electron collisions occur more rapidly than cation diffusion.

A small discontinuity in $n(x,1)$ occurs at $x=60-65$ due to a change in the treatment of cation collisions. For $x<60$ contributions from all cations with y between 1 and 60 are included in the calculation, but for $x>60$ it is assumed that this entire population of cations has $y=6$ and reacts at an effective rate equal to the previous sum. Thus, the discontinuity at $x=60-65$ is an artifact of a simplification in the calculation.

Turning now to experimental comparisons, as described in the Introduction silicon particle growth has been studied in a number of experiments, primarily at three laboratories. Unfortunately, two of these laboratories utilize silane highly-diluted in a noble gas [16,19]. The particle growth chemistry under those conditions, particularly at high powers where much of the silane is dissociated, is totally different than in the low power, silane, or silane-hydrogen discharges utilized to produce a-Si:H devices. In addition, they find that particle growth goes through an agglomeration stage, which does not occur for the discharge conditions of interest here.

In addition to the mass spectrometry measurements of negative ions described in Sec. III. Hollenstein *et al.* [15] have studied larger particles (>20-nm radius) in pure silane rf and VHF discharges by light scattering. They observe that after a delay of $\sim$50 s, a $2\times10^9\,cm^{-3}$ density of $r_p \approx 20$ nm particles suddenly appears and grows to over 40 nm within few seconds while the initial density drops by over an order of magnitude. The particle-growth rate and density attrition both then slow for the next 30 s. These observations

are similar to those of Ref. [16] and other studies from the Kyushu laboratory, although the long induction period is different. Agglomeration is clearly indicated, and probably occurs because densities of agglomerating particles exceed the cation density [20]. Since growth before agglomeration was not observed, the present theory cannot be compared to this data.

While the power and pressure conditions used by the Hollenstein group are similar to those used to obtain good quality *a*-Si:H devices, the small-particle densities are much larger than in Ref. [3]. We do not have a good explanation for this major difference.

At our laboratory we have studied particle growth in pure silane rf discharges at the low film-growth rates (0.1–0.4 nm/s) appropriate for device production [3]. We measured $r_p(t)$ and $n_p(r_p,t)$ for particles with $r_p=4-20$ nm versus time (t) after discharge initiation. We observed a nearly constant rate of r_p growth, except at very early times. Extrapolating from the observed growth of 4–20 nm particles back to discharge initiation indicates a slightly increased early growth rate, which is also seen in the present calculation and results from polarization forces between small charged particles and radicals. This linear growth rate is inconsistent with agglomeration during the observed growth from 4 to 25 nm radius, or by extrapolation even for smaller r_p. The present calculation is consistent with this, as significant agglomeration only occurs for plasma conditions that yield very-high-particle densities, at the right side of the data in Fig. 8.

To compare the calculations to Ref. [3] data we must relate the calculated, steady-state dn_p/dr_p to light scattering observations, which are most sensitive to the largest particles of a density distribution. It is reasonable to assume that the apparent $r_p(t)$ and $n_p(r_p,t)$ from the measurements represent a weighted average over a population of particles that start growth with equal probability at all times after discharge initiation. The distribution at time t after discharge initiation is then given by the integral of $n\{r_p(t-t_{\text{start}})\}$ over t_{start}, where $r_p(\tau)$ is the size and $n\{r_p\}$ the density of particles that have grown to for a time τ. This distribution is weighted by r_p^6, the Mie scattering cross section, and as shown in Ref. [3] this yields $(r_p)_{\text{apparent}}\cong 0.85(r_p)_{\max}$, where the maximum results from $t_{\text{start}}=0$, and $n_p(r_p,t)_{\text{apparent}} \cong 1\text{ nm}\cdot dn_p(r_p)/dr_p$ evaluated at $(r_p)_{\text{apparent}}$. Thus, the true particle-growth rate is 1/.85 times the apparent rate and the reported apparent density at r_p is close to the total/nm density at r_p reported here in Figs. 5, 7, and 8.

We will first compare to particle-growth rates in Ref. [3], but as this is a steady-state calculation additional considerations are needed. It is clear that the full time-dependent equation will yield a time delay $dt(x)$ associated with each x to $x+1$ step, where $1/dt(x)$ is the rate of removing $x+1$ particles. This removal rate, $M(x)_{z,z}$ in Eq. (1), must be weighted by the various $n(x)_z$ densities, but for $x>10^3M(x)_{z,z}$ is dominated by the radical-induced particle-growth rate that is nearly independent of z. Calculating $r_p(t)$ in this manner shows that it is linear in t for $r_p>1.3$ nm. The initial growth is more rapid, such that when $r_p(t)$ is extrapolated to $t=0$ it intercepts the axis at $r_p\cong 0.8$ nm. For $r_p>1.3$ nm, we obtain

$$dr_p dt = 44 L_e G (P/P_0)(\gamma_p/\gamma_f) \tag{3}$$

with L in cm, $P_0=1$ Torr$=133$ Pa, and γ_p and γ_f are the Si incorporation probability per SiH_3 reaction with the particle and the film surface. The particle-growth data in region *A* of Fig. 5 and the film-growth data in Fig. 9 of Ref. [3] can be combined to obtain $(dr_p/dt)/G$. When this is done, the G correction in the Ref. [3] citation, and the $\times 1.25$ correction between the apparent r_p in Fig. 5 and the maximum r_p is made, the lowest-pressure data (0.28 Torr) yields $(dr_p/dt)/G$ equal to $\sim$0.6 of Eq. (3) with $\gamma_p/\gamma_f=0.5$–1. This is excellent agreement, or it shows that $\gamma_p/\gamma_f\cong 1$, but the measured $(dr_p/dt)/G$ ratio rises with P and reaches $\sim$1.5 times Eq. (3) at the highest pressure of 0.4 Torr. This is still reasonable agreement with Eq. (3), but it is clear that something not included in the present theory occurs at the higher P. The higher power data in region *B* of Fig. 5 of Ref. [3] further requires this, as it represents a $(dr_p/dt)/G$ ratio several times that given by Eq. (3).

One possible cause of the increased $(dr_p/dt)/G$ ratio described in the previous paragraph is that γ_p/γ_f changes. This could result from different particle interactions with particles versus film; for example, ion bombardment of the film is much more energetic than for the particles, particularly at lower P. This could increase the film reactivity and thereby γ_f at lower P, consistent with the observed trend in $(dr_p/dt)/G$. Another possibility, suggested in Ref. [3], is that as P and G increase heavier radicals make an increasing contribution to both film and particle growth; these diffuse more slowly to the surface, yielding increased density in the plasma versus flux to the film. However, we note here that heavier radicals also collide less frequently with particles due to a lower velocity, and when both factors are taken into account the net difference is minor compared to SiH_3. A third possibility appears most probable, and is consistent with the higher-radical densities in the present calculation. Radical-radical collisions that yield stable molecules lower the radical flux to the surfaces relative to radical density in the central region where they are formed. This will raise the ratio of particle growth and/or film growth, and it occurs at higher P and G values where the calculation yields a large fraction of higher radicals, consistent with the experiment. This decrease in radical flux to the electrodes also modifies the relationships between G, $n(1,0)$, and n_e, given in Appendix A and Eq. (2). Including this would somewhat increase the larger-particle densities in Fig. 8, but the additional complication to the calculation does not appear justified in view of the many rate-coefficient uncertainties.

As noted in Ref. [3], and is apparent from Eq. (3), one can approximately calculate the particle-growth rate without the present model. The real test of this model is the measured particle density versus conditions. For this comparison the $r_p=8$ nm, particle-density data in Fig. 7 and G data in Fig. 9 of Ref. [3] can be combined to yield apparent $n_p(r_p=8\text{ nm})$ versus G and n_S at $L=1.5$ cm. As noted earlier in this section, the calculated total/nm particle density at r_p is close to the apparent measured density at r_p, so we have plotted the experimental n_p $(r_p=8\text{ nm})$ in Fig. 8. There the theoretical points correspond to $r_p\cong 4$ nm, and somewhat lower values would occur for $r_p=8$ nm for the lower-density points. Nonetheless, it can be seen that the data follows the

same pattern as the theory, and that the range of n_S and G values studied in the experiment yield a consistent pattern when plotted versus the $n_S^{0.6}GL^{1.5}$ abscissa of Fig. 8. This is a strong indicator of the validity of this scaling parameter.

In addition to the general scaling behavior, the theoretical points are very close to the data in Fig. 8; even closer if the theory points are lowered to represent $r_p=8$ nm. No adjustments of rate coefficients have been made to obtain this near agreement, and this is a coincidence. As described in Sec. III, the uncertainties in many rate coefficients are large enough to yield a factor of 2 horizontal shift of the theory in Fig. 8. In addition, recall from Appendix A that k_d and thereby n_e is uncertain by perhaps a factor of 3, and may have considerable dependence on G, which is not included in the theory. It was also noted earlier in this section that n_e is probably higher for the higher n_p in Fig. 8, due to radical-radical collisions that lower G relative to silane dissociation. It is also quite likely that radical-radical collisions are more effective at producing higher-x radicals than has been assumed. The appearance of Si_3H_8 and Si_4H_{10} as first-order products of silane dissociation and subsequent radical-silane reactions demonstrates the chains of radical-silane reactions that can occur [12].

One additional comparison to experiment can be made using Ref. [2] where particle incorporation into films was measured. In Fig. 7(b) particle flux$\cong 10^{13}x^{-2}$/s cm^2 in the $x=10^3-10^5$ range, and as each particle carries x Si atoms to each of two surfaces, the total atom flux to one surface is $10^{12.7}x^{-1}$/s cm^2. The flux of Si atoms from particles with size between x_0 and x_1 is thus $F(x_0)=10^{12.7}\int_{x_0}^{x_1}dx\,x^{-1}$/s cm$^2=10^{12.7}\ln(x_1/x_0)$/s cm^2, and for $x_0=10^3$ and $x_1=10^5$, corresponding to the range of particle sizes observed in films in Ref. [2], $F(x_0)\cong 2\times 10^{13}$/s cm^2. For Fig. 7(b) $G=2$ Å/s, or 10^{15} Si atoms/s cm^2, so for these conditions the Si atoms deposited in these particles is $\sim 2\%$ of the film volume. Figure 7(a) shows that when G decreases about a factor of 2 this flux decreases by $\sim 10^4$, and in Fig. 7(c) it increases by a similar factor. [For the particle density of Fig. 7(c), which is far above the experimental densities, the total Si consumed by growing particles greatly exceeds that going into film.] In comparison, in Ref. [2] where the deposition of $R_p=2-8$ nm particles onto the growing film was detected, these represented $10^{-3}-10^{-4}$ of the film volume. The experimental n_S, L, and G that yielded this fraction are close to the range of parameters in Ref. [3], although $T=520$ K in Ref. [2]. Thus, as in the comparison to Ref. [3], the theory is well within the expected range of agreement with Ref. [2]; at most a factor of 2 translation along the abscissa of Fig. 8 is required.

V. CONCLUSIONS

The purpose of this paper is to establish a quantitative basis for understanding particle growth and densities in silane discharges. This has required establishing reasonable values for many different types of collisional rate coefficients, all versus the number of Si atoms in one or both colliding species. In doing so many assumptions and approximations have been made, and the rationale for these has been explained. We are certain that many improvements and corrections to these can be argued or will appear some day, but we believe that the general pattern of $r_p=3.6$ nm particle density (n_4) versus plasma parameters P, L, and G seen in Fig. 8 will remain. However, the actual values of these three parameters where a particular n_4 occurs, or perhaps the curvature in n_4 versus the abscissa in Fig. 8 will change.

Although the L dependence was not measured, the data of Ref. [3] groups together in Fig. 8 when plotted versus the combination of parameters that also groups the theoretical results. The value of this $P^{0.6}GL^{1.5}$ parameter that yields theoretical particle densities is also close to the experimental value. Although such close agreement is a coincidence, it indicates that the basic character and causes of Si particle growth in pure silane discharges has been explained here. The techniques and rate coefficients reported here can also be used to develop understanding of particle growth in silane mixtures with H_2, argon, and other gases.

There have been several other interesting results from the calculation besides visible particle densities. One is the rather large contribution of higher radicals (containing more than one Si atom) to both film and particle growth. This results from radical-radical reactions, and it is most extreme as the plasma parameters move to the right in Fig. 8. Actual values of film growth due to all radicals (G) versus only SiH_3($G1$) are given for several cases in Table I. This increasing fraction of film growth from higher radicals, with increasing G, may have important implications for film quality.

Another, perhaps surprising, result is that in this neutral plasma region where particles reside, the electron density is normally 100–300 times smaller than the cation and anion densities. As has been described above, this is the cause of the very large neutral fraction of particles, and thus for the large particle flux to the substrate under conditions where $n_4>10^4$ or so in Fig. 8.

One clear conclusion from this work is that if ''large'' particles (e.g., with greater than 10^3 Si atoms) are deleterious to a-Si:H devices, then the only way to avoid a large flux to the electrodes is to keep the abscissa of Fig. 8 ($N^{0.6}L^{1.5}G$) below a critical value. On the other hand, it may be possible to direct this particle flux to only one electrode or particular regions of either electrode, and thereby keep them out of the a-Si:H device. Some methods that might achieve this have been discussed in Ref. [18]. However, these methods do not prevent the higher radicals from incorporating into films.

ACKNOWLEDGMENTS

This work was supported in part by the National Renewable Energy Laboratory, under Contract No. DAD-8-18653-01. I also wish to thank A. V. Phelps and M. A. Childs for valuable suggestions.

APPENDIX A: DENSITIES OF $X=1$ PARTICLES

Since SiH_3 diffuses without reacting with silane and is produced primarily within the central $\frac{2}{3}$ of the electrode gap, it assumes a nearly fundamental-mode spatial distribution, $n(Z)=n_c\sin(\pi Z/L_D)$, where $n(Z)$ is an abbreviation for $n(1,0)$ versus Z and n_c is the value midway between the electrodes. Z is the distance from slightly behind one elec-

trode, since L_D typically exceeds the electrode gap L by ~10% due to the boundary condition [3]. (Corrections in this distribution due to radical-radical reactions are not included in the present calculation.) The SiH_3 flux to each surface is $D_1 dn/dZ = D_1 n_c \pi / L_D$ at $Z=0$ and L_D, where $D_1 \equiv R(1,0)_D$ is the SiH_3 diffusion coefficient. It is assumed that each SiH_3 reaction with the film surface incorporates an average of 0.4 Si atoms in the film [21,22]. Thus, $n_c = G_1 \rho L_D / 0.4 \pi D_1$, and ~90% of this will be used as an average across the neutral plasma region where particles reside,

$$n(1,0) = 0.8 G_1 \rho L / D_1 . \tag{A1}$$

A typical value for $G_1 = 2$ Å/s, $n_S = 10^{16}/\mathrm{cm}^3$, and $L_D = 1.5$ cm is $n(1)_0 \cong 5 \times 10^{12}/\mathrm{cm}^3$.

The contribution of all radicals to particle growth is taken into account in the calculation by using Eq. (2) for G, and equivalently $0.4 \Sigma x n_x k_x$ is the total radical rate of Si-atom attachment to particles.

The dominance of dissociation in producing film growth in low-power, pure-silane discharges is well established [12]; the primary mechanism is that each SiH_4 dissociation yields approximately two SiH_3 radicals from H-atom reactions with SiH_4. (In addition, it yields about one Si_2H_6 molecule from SiH_2 reacting with SiH_4.) Thus, we assume that each dissociation yields two SiH_3 molecules, that each of these produces 0.4 Si atoms in the film, and that the dissociation rate per cm^2 of electrode area is $R_d = n_e k_d n_S L'$ where k_d is the dissociation rate coefficient and L' is 70% of the electrode gap. The rate of SiH_3-induced Si deposition per cm^2 of discharge is $2 \rho G_1$, where ρ is the film silicon density ($5 \times 10^{22}/\mathrm{cm}^3$), and G_1 the growth rate on one electrode. The n_e required to yield G_1 is thus

$$n_e \cong 2.5 \rho G_1 / k_d n_S L' . \tag{A2}$$

Using the measured dissociation cross section, rf discharge models have provided a range of values for k_d that vary about a factor of 3 from a nominal value of $10^{-9}\ \mathrm{cm}^3/\mathrm{s}$, where the variations depend on discharge conditions and model assumptions [23,24]. Using this nominal value, which has an uncertainty of $\sim 3x$. A typical value, for $G = 2$ Å/s, $n_S = 10^{16}/\mathrm{cm}^3$, and $L = 1$ cm, is $n_e \approx 10^8/\mathrm{cm}^3$.

This paragraph explains the anion and cation densities that occur in the neutral plasma region. Since anions cannot escape the plasma, the total anion charge density (n_-) will reach steady state when this charge is being removed at the rate new anions are being formed. The latter is principally SiH_3^- production by electron collisions with silane, at a rate per unit volume $R_{\mathrm{att}} = n_e k_a n_S$ where k_a is the dissociative-attachment rate coefficient. Anion charge can be removed by electron collisions, but as pointed out by Perrin [11] this is much slower than anion-cation mutual neutralization in these discharges. Thus, charge neutralization by positive ions essentially equals R_{att}. As anions build up in the discharge, cation density keeps pace to yield a nearly neutral plasma and this buildup stops, typically in ~1 ms, when mutual neutralization balances SiH_3^- production. In steady state the total cation density (n_+) greatly exceeds n_e, so in essence $n_+ = n_-$. This calculation shows that cation charge is dominated by $x < 100$ and anions by $x < 200$, so recombination of light cations and anions essentially balances R_{att}. The recombination of this distribution of $Si_yH_j^+$ and $Si_xH_m^-$ should be summed over x and y to obtain the total recombination rate, and this is done in the full calculation using an x,y-dependent $k(x,y)_{II}$. However, this mutual neutralization rate coefficient is not very sensitive to x and y within this range, and a fairly good estimate is obtained with a single, average value of $k_N = 8 \times 10^{-8}\ \mathrm{cm}^3/\mathrm{s}$. This yields a particle charge neutralization rate of $n_- n_+ k_N = (n_+)^2 k_N$, and overall

$$n_+ \cong (n_e k_a n_S / k_N)^{1/2}, \tag{A3}$$

where n_e can be obtained from Eq. (A2). A typical value for $G = 2$ Å/s, $n_S = 10^{16}/\mathrm{cm}^3$, and $L = 1.5$ cm is $n_+ \cong 2 \times 10^{10}/\mathrm{cm}^3$.

APPENDIX B: RATE COEFFICIENTS AND RATES

1. Electron collisions

The cross sections for electron collisions with SiH_4, resulting in elastic, inelastic, ionizing, and dissociating processes, have been measured or inferred from swarm measurements [11]. In the rf discharge, cycle, and volume-averaged rate coefficients for collisional dissociation (k_d) and dissociative attachment (k_a) are needed to model particle growth. Models for these discharges [23,24] have provided effective rate coefficients for discharge conditions fairly close to those of interest here. We will use nominal values, $k_d = 1 \times 10^{-9}\ \mathrm{cm}^3/\mathrm{s}$ and $k_a = 8 \times 10^{-12}\ \mathrm{cm}^3/\mathrm{s}$, in the center of the model results and close to the values recommended by Perrin [11]. The present calculation is only sensitive to the ratio k_a/k_d, which is relatively insensitive to rf power and pressure because both processes have a threshold near 8 eV.

Electron collisions with particles are a very important but little-studied aspect of particle charging, so we will discuss it in considerable detail. These collisions can lead to attachment, decreasing z by 1, or to electron detachment (a secondary electron), increasing z by 1. But as noted in Appendix A this detachment makes a much smaller contribution to raising z than cation attachment, so we delete it in the calculation, taking $R(x,z)_{\mathrm{ED}} = 0$.

Electron attachment to a negatively charged particle requires that the electron kinetic energy (E_e) be sufficient to overcome the surface potential $\phi(x,z) = zq/4\pi\varepsilon_0 r_p = E_0 z (5.9/x)^{1/3}$. This leads to the well-known orbit-limited electron current to the particle $i_e = q \pi r_p^2 \langle v_e \rangle n_e \exp(-q\phi/kT_e)$ [1]. This describes the rate of electron collisions with a particle, but in order to attach to the particle the electron must lose kinetic energy within the particle, as indicated diagrammatically in Fig. 9. This is also true for attachment to a neutral particle; the only difference is the lack of a barrier outside the particle. Inside the particle the electron suffers a combination of elastic scattering by irregularities within and at the surface of the particle, and inelastic scattering due to excitations of particle phonons, SiH bonds, and electron-hole pairs. Trapping an electron within a crystal Si (c-Si) particle is more difficult than in a a-Si:H particle because the mean free path for scattering (λ_S) is much larger in the former material. (The degree of

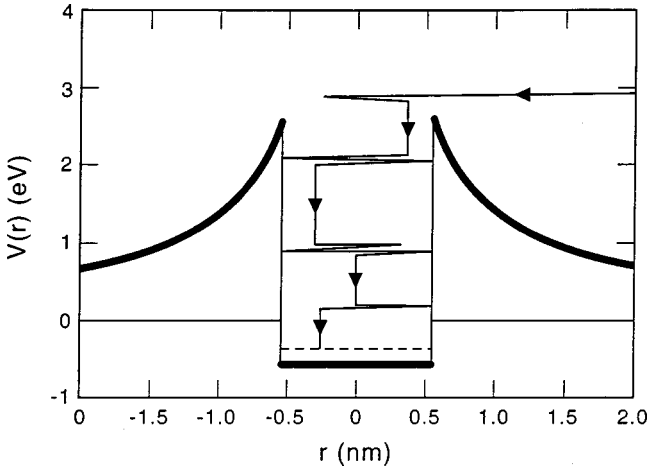

FIG. 9. Diagrammatic representation of electron capture by a particle (the path with arrows) due to elastic scattering combined with inelastic scattering, primarily by forming electron-hole pairs that stabilize by radiative recombination and phonon coupling. The dashed line is the ground state for one captured electron.

crystallinity may depend on power as well as the gas temperature.)

In *a*-Si:H, elastic scattering from Si disorder occurs with $\lambda_S \approx 0.5$ nm for electron energies E_e near the conduction-band edge, and about 1 nm might be expected for 3-eV higher E_e (i.e., $Q_{\text{scatt}} \sim 2\times10^{-16}\,\text{cm}^2$). Bulk *a*-Si:H film typically contains H:Si$\approx$0.3 at 300 K, and 0.1 at 530 K where device films are normally made. The SiH vibrations have 0.25-eV stretch and 0.078-eV wag modes that are infrared active, indicating a strong dipole moment. Electron excitation of these vibrations will relax E_e, probably with a cross section of $\sim5\times10^{-17}\,\text{cm}^2$ at $E_e = 2-4$ eV, which is the measured vibrational excitation cross section per H atom in SiH_4 and Si_2H_6. (This yields a mean free path for vibrational excitation $\lambda_v = 13$ nm for H:Si$=0.3$.)

Ionization, the creation of an electron-hole pair, has an effective threshold of $\sim$1.5 times the band gap E_G, and it has been suggested in ballistic-electron studies that in GaP the mean free path for ionization, or electron-hole formation, is $\lambda \sim 10\text{ nm}\,(E-E_{\text{th}})^2E^{-1/2}$ with energies in eV units [26]. Assuming this also applies to these Si particles, that $E_G \sim 1.6$ eV as in *a*-Si:H or a somewhat quantum-confined small *c*-Si particle, and taking $E = A_e + E_G \cong 5$ eV in the above relation yields $\lambda_{\text{ion}} \sim 3$ nm, where A_e is the electron affinity. The probability (P_1) that the electron causes an ionization event before exiting a spherical particle is a complicated problem of random scattering and relaxation, which we will not do here although some more exacting, related work exists [27]. Instead, a rough estimate will be obtained by considering the character of one-dimensional diffusion with reactions. The probability of traversing a distance x without an ionization (the reaction) is $\exp(-x/x_0)$, where $x_0 = (\lambda_S\lambda_{\text{ion}}/3)^{1/2} \approx 1$ nm. (The characteristic distance for N ionizations is $N^{1/2}$ times this.) Of course, this diffusion solution does not apply to a particle that is smaller than λ_S; the average straight-line traversal length is then $\sim 1.6r_p$, yielding an ionization $P_1 = 1.6r_p/\lambda_{\text{ion}} = r_p/2$ nm for $r_p < \lambda_S$.

Ionization removes 1–2 eV from E_e, temporarily stabilizing the electron in the particle. However, this can be reversed by electron-hole recombination accompanied by ejection of the extra electron; essentially Auger ionization. Radiative electron-hole recombination and vibrational or phonon excitation compete with Auger ejection, to yield attachment for a fraction of ionization events. For simplicity we assume that this fraction is 1, and test the effect of a smaller value in Sec. III. It is also likely that a significant fraction of electrons will scatter from all particles, so for all x we take an attachment probability $P_a = 0.7P_1$. These considerations suggest an attachment probability of $P(x)_a = 0.7[1-\exp(-a/1.5\text{ nm})] = 0.7[1-\exp(-x^{1/3}/9)]$. Note that $P(1)_a \cong 0.07$ and $P(x)_a$ approaches its high-x limit for $x \sim 10^3$.

For $x < 50$ a molecular picture seems more appropriate for electron attachment. Electron attachment to a molecule is normally stabilized by dissociation, and in the present case of Si_xH_m molecules H or H_2 detachment should dominate. A relevant example is the SiH_4 dissociative attachment to form SiH_3^-, which starts the negative ion growth process. The rate coefficient for this process, $k_a = 8\times10^{-11}\,\text{cm}^3/\text{s}$, represents an attachment probability of $\sim 3\times10^{-4}$ per collision by all electrons, and $\sim 3\times10^{-2}$ for electrons with the $\sim$8 eV required to excite the dissociating state. As x increases, the required excitation energy should rapidly drop, and the cross section at this energy should increase at least as fast as x. Based on this, a reasonable approximation for P_a would appear to be $P(x)_a = 0.7[1-\exp(-4\times10^{-4}x^{\gamma})]$ with $\gamma = 1-2$. This yields $P(1)_a = 3\times10^{-4}$ and the high-x limit is approached at $x = 50$ (or 2500) for $\gamma = 2$ (or 1). To obtain the previous ''solid'' result of approaching the high-x limit at $x \cong 10^3$, and the ''molecule'' result at small x, we will use

$$k(x,z)_{\text{EA}} = \pi R_p^2 \langle v_e \rangle n_e \exp[-\phi(x)/T_e] P(x)_a ,$$

where

$$P(x)_a = 0.7\{1-\exp(-4\times10^{-4}x^{\gamma})\}. \tag{B1}$$

We will nominally use $\gamma = 1$, but will also test the sensitivity to varying $P(x)_a$ in the critical $30 < x < 10^3$ region. This rate coefficient is plotted in Fig. 1, and the rate $R(x,z)_{\text{EA}} = n_e k(x)_{\text{EA}}$ is plotted for typical conditions in Fig. 2.

This $k(x,z)_{\text{EA}}$ is obviously quite uncertain, but electron attachment is most significant in the calculation for $x > 30$, and for $x > 10^3$ a high probability of attachment appears reasonable. Thus, this is a significant but not overpowering uncertainty.

2. Cation-particle collisions

Collisions of singly charged positive ions, $Si_yH_n^{+1}$, with negatively charged particles, $Si_xH_m^{-N}$, are normally described by orbit-limited current (OLC) theory [1], which obtains the neutralization rate coefficient

$$\begin{aligned} k(x,z)_N^{\text{OLC}} &= v_r \pi r_p^2 (1 + q\phi/kT_+) \\ &\cong v_+ (1+y/x)^{0.5} \pi z (E_0/kT_+) r_p \times 1 \text{ nm}, \end{aligned} \tag{B2}$$

where v_r is the relative velocity and v_+ the ion velocity, and we will use $kT_+ = k(300\text{ K}) = 0.026$ eV except as noted. In

the second part of Eq. (B2) we used $q\phi = E_0 z(\mathrm{nm}/r_p)$ and $q\phi/kT_+ \gg 1$. As is customary, the cation radius $a(y)_+$ was neglected compared to r_p in Eq. (B2). For the small particles of interest here it can be significant, and yielding

$$k(y,x,z)_N^{\mathrm{OLC}} = v_1(y^{-1}+x^{-1})^{0.5}/\pi z(E_0/kT_+) \times [r_p + a(y)_+]^2(1 \ \ \mathrm{nm}/r_p), \qquad \text{(B3)}$$

where v_1 is the SiH_4 velocity.

The OLC theory assumes that the particle and ion remain charged throughout their orbit and must make contact to undergo a collision. However, for small x and y an electron jump often occurs at a larger radius due to a level crossing between the ion-pair potential and an excited state of the neutral complex. This charge-transfer mechanism, sometimes called ''harpooning,'' was used by Hickman (and others previously) to describe mutual neutralization of small molecules [25]. Hickman fitted a large number of mutual-neutralization reactions by, in essence, assuming that the electron jump occurred at a radius $r_C \cong 0.9\ \mathrm{nm}\,(\mathrm{eV}/A_E)^{0.4}$, where A_E is the electron affinity of the negative ion. This yields the k_N of Eq. (B3), but with $r_p + a_+$ replaced by r_C whenever the latter is larger. As can be seen from the change of slope of $k(x,-L)_N$ in Fig. 1, for the $y=6$ cation this occurs for $x<16$ and yields a maximum difference of about a factor of 2 at $x=1$. For particles with $-zq$ charge we multiply this rate coefficient by $|z|$, but since multiple charges only occur for $x>60$ the r_C correction only applies to $z=-1$.

The average cation in the calculation has $y=6$. Compared to $y=1$ (SiH_3^+) this raises $a(y)_+$ in Eq. (B3) by $\sqrt{6}$ and lowers the cation contribution to v_r by $\sqrt{6}$, so overall it does not have a major effect on the ion-attachment (or ion-ion recombination) rate coefficient $k(x,z)_{\mathrm{IA}}$. These coefficients for $y=6$ and $z=-1$, -2, and -3 are plotted as $k(x,z)_{\mathrm{IA}}$ in Fig. 1, and the rates $R(x,z)_{\mathrm{IA}} = k(x,z)_{\mathrm{IA}} n_+$ are plotted for typical conditions in Fig. 2.

A collision between a cation and a negatively charged particle could yield charge transfer to the ion without attaching to the particle. Here we will provide reasons for deleting this process. First, the ions have at least one dangling Si bond and are reactive even without their charge. Thus, it appears likely that if they contact the particle they will insert into a Si-H bond and attach. For the $r_C > r_p + a_+$ region described in the previous paragraph, a fraction $f = [1-(r_p + a_+)/r_C]^2$ of the orbits yield a charge transfer without contact, and thereby without attaching the cation. This is a significant fraction of ion collisions only for $x<10$, and for $x<6$ particle growth by SiH_4 collisions is much faster than by ion or radical collisions. Thus, the distinction between anion-cation neutralization with or without attachment has no practical consequence for small x. In addition, since radical-induced growth greatly exceeds ion-induced growth at all x, this distinction is never important. By setting $R(y,x,z)_{\mathrm{IA}} = n_+ k(y,x,z)_N^{\mathrm{OLC}}$ and $R(x,z)_{\mathrm{EX}} = 0$ (EX is the electron exchange) the full neutralization rate is obtained while simplifying the particle-growth equations.

The above paragraph treated cation attachment to negatively charged particles, obtaining a rate proportional to z that is 0 for a neutral particle. Here we treat cation attachment to a neutral particle. The dominant interaction between an ion and neutral particle is the polarization potential, $V(R) = -C/2R^4$, where $C = (q^2/4\pi\varepsilon_0)\alpha$ and $\alpha \cong (4\pi r_p^3/3)$ is the particle polarizability since the particle index of refraction is much greater than 1. This leads to the familiar Langevin rate coefficient for ion-molecule reactions

$$k(x,0)_{\mathrm{IA}} = 2\pi(C/2M)^{1/2} \cong (8\times 10^{-11}\ \ \mathrm{m}^3/\mathrm{s})(r_p/\mathrm{nm})^{3/2} \qquad \text{(B4)}$$

where M is the reduced mass and IA is the ion attachment. The second expression applies for an ion mass of $y=6$ and a much larger-particle mass, as is appropriate for the calculation. When r_p exceeds the effective orbiting-capture radius, $k(x,0)_{\mathrm{IA}} = v_+ \pi r_p^2$, so we add this hard-sphere value to that in Eq. (B4) for the total rate coefficient. This total rate coefficient, for $y=6$, is shown in Fig. 1, and the rate $R(x,0)_{\mathrm{IA}} = k(x,0)_{\mathrm{IA}} n_+$ is plotted for typical conditions in Fig. 2.

3. Charged-particle collisions with SiH_4

As noted in Sec. II B, the growth of negatively charged particles must compete with neutralization by cation attachment, followed by particle diffusion to the surfaces. For small x this diffusion is very fast and almost all particle neutralization results in particle loss. Thus, the fraction of initially formed SiH_3^- that survive to become large and observable is very sensitive to the growth rate from $x=1$ to 100. The anion measurements of Hollenstein, Howling, and associates [28] suggest that this growth rate is very fast due to collisions with SiH_4, so this is very important to modeling particle growth. By collecting anions $Si_xH_m^{-1}$ with $x=1-40$ in the afterglow of a pulsed discharge, they have clearly established that initial ion growth must occur through the process

$$Si_xH_m^- + SiH_4 \rightarrow Si_{x+1}H_m^- + (\mathrm{H\ or\ H_2})\ \ \mathrm{products} \qquad \text{(B5)}$$

In essence, $x \rightarrow x+1$ growth occurs much more rapidly than collisions with SiH_n radicals or cations, so no other explanations of the data are possible. They have deduced a rate coefficient of $k(x,-1)_S \cong 3\times 10^{-12}\ \mathrm{cm}^3/\mathrm{s}$ for small x, and one interpretation of the data suggests that this value may apply from $x=1-40$. However, for the discharge modulation reported the observed heavier ions may have accumulated in the reactor over many discharge cycles, so another interpretation is that $k(x,-1)_S \cong 3\times 10^{-12}\ \mathrm{cm}^3/\mathrm{s}$ for $x<\sim 6$, but $k(x,-1)_S$ has not been established for $x>\sim 6$. Consequently, we will estimate an effective value of x, where $k(x,-1)_S$ starts to decrease, from the following reaction model.

Since SiH_4 does not react significantly with the growing a-Si:H film and the particles are expected to have a very similar structure and surface H coverage, we do not expect SiH_4 to react with the larger particles. In fact measured particle growth rates require this for the $r_p > 4$ nm particles that were observable by light scattering [3]. One major difference between a SiH_4 collision with a charged particle versus the a-Si:H film is the electric field around the particle. This polarizes the SiH_4 molecule, leading to the interaction potential $V(R)_S = -C_S/2R^4$, where $C_S = |z|(q^2/4\pi\varepsilon_0)\alpha_S$ and α_S

$=4.6\,\text{Å}^3$ is the polarizability of SiH_4 [11]. This yields, for SiH_4 (radius $a_S \cong 1.5\,\text{Å}$) at the particle surface where $R = r_p + a_S$, $V(R_S)/kT = -160z(x^{1/3}+0.9)^{-4}$ for $T = 300$ K. For $z=1$ this ratio equals 1 at $x=19$.

Another way to estimate the binding energy E_B of a SiH_4 to a negatively charged particle is to equate it to $d(A_E)/dx$, where the electron affinity A_E is given in Appendix C. This yields $E_B/kT = 38x^{-4/3}$, which is similar to the previous expression in the $x=5-30$ region of interest, and equals 1 for $x=15$. This additional binding energy can enhance the ability of SiH_4 to bond to the particle, both by increasing the surface residence time and by partially overcoming the reaction barrier. The reaction of a surface Si-H bond with a SiH_4 Si-H bond, to yield a Si-Si bond plus H_2, is on average exothermic by ~ 0.2 eV, but a considerable reaction barrier is expected since SiH_4 does not react efficiently with *a*-Si:H surfaces below ~ 1500 K [29]. Thus, it is not apparent if this extra impact and binding energy can provide a plausible explanation of reaction (B5). However, it is interesting that this fractional enhancement decreases with increasing T, consistent with the familiar observation of fewer particles at elevated temperatures.

Using the previous paragraph as a guide, the calculation will use a $k(x,-1)_S$ that decreases with increasing x, using a parameter (A) to adjust the falloff rate:

$$k(x,-1)_S = k_0[1-\exp(-Ax^{-4/3})], \tag{B6}$$

with $k_0 = 3\times 10^{-12}$ cm^3/s. This is shown for $A=10$ and 100 in Fig. 1, and the typical rate, $R(x,-1)_S = k(x,-1)_S n_S$ is in Fig. 2.

Reactions of $Si_xH_m^+$ cations with SiH_4 have been reviewed by Perrin [11]. Most of these reactions are very rapid for $x<3$, but they decrease rapidly for higher x and are too small to be observed for $x>6$. Both the reaction rate coefficients and the products are sensitive to m as well as x, and in many x,m cases the charged reaction products are not known. Of course, neutral radical reaction products are not measured for any x,m case. Thus it is not feasible to keep track of all x,m cations or the radicals that might also result, and this would immensely complicate the present calculation if it were possible; major approximations are required. Some cation reaction products have added the Si from the SiH_4 and some have not, but few split into smaller x than the initial cation. It therefore seems reasonable to take an m-independent rate coefficient for adding one Si, $k(x,1)_S$, that smoothly and rapidly decreases from $y=3$ to 6, while neglecting any collision-induced decrease in y. The first step is dominated by $SiH_3^+ + SiH_4$ since SiH_2^+ rapidly converts to SiH_3^+ and the other SiH_n^+ products of electron collisional ionization are minor. Thus, the calculation starts with this measured value as $k(1,1)_S$ and multiplies this by $\exp(-x/4)^4$ to smoothly terminate it by $x=6$. This $k(x,1)_S$ is shown in Fig. 1, and the resulting rate for typical conditions is in Fig. 2. As will be seen below, this leads to an average cation mass of $x\sim 6$.

4. Radical-radical collisions

Since particles are represented only by the number of Si atoms, a collision between neutral particles (radicals) with x and y Si atoms will yield product particles with x' Si atoms. The rate coefficient versus x' should represent an average over the range of products that result from a mixture of Si_xH_m and $Si_yH_{m'}$ collisions. For small x and y the expected x' distribution is quite complex, and most of it must be guessed in any event since data is not available. For large x or y it may be simpler, but some major approximations are still required. For large-x particles, the important collisions are with light ($y<10$) radicals. We have already indicated above that at the *a*-Si:H film we will assume that Si_yH_m radicals incorporate with a probability (P_r) that is independent of y and m, and that this incorporation attaches y Si atoms. Since a large-x particle should have essentially the same surface as the film, it is reasonable to make the same assumption for incorporation of Si_yH_m into a large-x neutral particle. Thus, for large x and small y, the rate coefficient $k(x,y)_{RR}$ for growth to a particle with $x+y$ Si atoms is $P_r k_{HS}(x,y)$, where $k_{HS}(x,y)$ is the 300 K, hard-sphere rate coefficient. (The subscript RR refers to radical radical)

$$\begin{aligned} k(x,y)_{RR} &= P_r v_{rel}\pi(r_p+a_y)^2 \\ &= P_r 4\times 10^{-11}\{(x+2)^{1/3}+(y+2)^{1/3}\}^2 \\ &\quad \times[(x+y)/xy]^{1/2}\ \text{cm}^3\,\text{s}^{-1}, \end{aligned} \tag{B7}$$

where v_{rel} is the relative velocity, r_p is the heavy-radical, and a_y is the light-radical radius. This is shown versus x for $y=1$ in Fig. 1, and the resulting rate $R(x,1)_R$ is in Fig. 2 for typical conditions.

The other important radical-radical collisions are those with $x=1-10$ and $y=1-10$, as these determine the mixture of small radicals. Radical-radical collisions are very exothermic, so they are expected to occur with gas-kinetic rates and indeed do so where they are measured. However, there are many possible product radicals, many of which are expected to rapidly react with one or more SiH_4, adding Si atoms but sometimes producing a stable higher silane. The overall effect should be to increase radical size part of the time, by producing a mixture of $x'>x$ or y radicals. In the most important case of the SiH_3+SiH_3 reaction, one product (SiH_2+SiH_4) yields only stable gases, while Si_2H_m+H and H_2 with $m=2-5$ yields $x'=2$ and 3 radicals (some after radical-silane reactions), often accompanied by an additional SiH_3 after the H reacts. Thus, it appears as reasonable as anything else to assume that the average effect per gas-kinetic collision is that a fraction P_r of all reactions leads to $x=x+y$ and all others have no effect. The obvious advantage of this simplification is that it is the same assumption used above for $x \gg y$, so Eq. (B7) applies for all x and y.

As already noted, in the calculation we use the same probability P_r for Si incorporation into particles and film. As long as this is done the results are largely independent of the actual value of P_r. The visible-particle growth rates observed in Ref. [3] at low P and G are consistent with this assumption of a similar P_r for film and particles, although changes occurred at the higher P and G studied where higher radicals and radical-radical collisions are important. We therefore assume this here, taking $P_r = 0.4$ from measured SiH_3 incorporation probability into *a*-Si:H film [21,22]. (Note that this is the probability of Si incorporation per reaction, not the reaction probability per surface collision.)

5. Ion-radical collisions

The long-range SiH_3 interaction with a (zq) charged particle is essentially the same as that of SiH_4, described in Sec. 3 of this Appendix. The resulting Langevin rate coefficient is

$$k(x,z)_L = 2\pi(C_R/2M)^{1/2}, \tag{B8a}$$

where M is the reduced mass, $C_R = |z|(q^2/4\pi\varepsilon_0)\alpha_R$ and $\alpha_R = 4.6\,\text{Å}^3$, the polarizability of SiH_4, is assumed. For Si_yH_m radicals with $y>1$ the radical polarizability and mass are both approximately proportional to y, so the same $k(x,z)_L$ is used. When the particle radius greatly exceeds the effective radius for orbiting capture, the hard-sphere cross section [Eq. (B7) without the P_r factor] applies, and is added to the Langevin k to obtain a $k(x,y,z)_{\text{IR}}$ that is reasonably valid for all x,y,z,

$$k(x,y,z)_{\text{IR}} = k(x,z)_L + k_{\text{HS}}(x,y). \tag{B8b}$$

This rate coefficient is plotted versus x in Fig. 1 for $y=1$ and $z=-1$ and -2, and the rate $R(x,-1,z)_{\text{IR}} = k(x,1,-1)_{\text{IR}}n(1,0)$ is plotted for typical conditions in Fig. 2.

6. Diffusion rates

The neutral-particle diffusion rate will be taken as the fundamental-mode rate for particle diffusion in silane, which is $R(x,0) = D(x,0)(\pi/L_D)^2$, where $D(x,0)$ is the diffusion coefficient, $L_D = L + 2\Delta L$, L is the electrode gap, and $2\Delta L$ is a small added length due to a finite density at the boundary. Except for $x<3$ at low L and P, $2\Delta L$ is insignificant and it will be deleted below. (An experimental L_D should be matched to the L used in this model.) $D(x,0) = \lambda(x)v(x)_r/3$ is used, where $\lambda(x) = (Q_{x,0}n_S)^{-1}$ is the $(z=0)$ particle mean free path between silane collisions $v(x)_r = v_S(1+x^{-1})^{0.5}$ is the relative velocity, and v_S the silane velocity. With $Q_{x,0} = \pi(r_p + a_S)^2$ the overall result is

$$\begin{aligned} R(x,z=0)_D &= (\pi/3)v_S(1+x^{-1})^{0.5}L^{-2}(r_p+a_S)^{-2}n_S^{-1} \\ &= 1.7\times10^4\ \text{s}^{-1}(1+x^{-1})^{0.5} \\ &\quad\times[(x+2)^{1/3}+1.4]^{-2}L^{-2}N_S^{-1}, \end{aligned} \tag{B9}$$

where $N_S = n_S/(10^{16}/\text{cm}^3)$ and n_S is the silane density.

Cations drift rapidly to the electrodes once they enter the sheaths, which typically extend ~20% of the electrode gap from each electrode. If one assumes no electric field within the ''neutral plasma'' region, then $R(x,1)_D = D(x,1)(\pi/L_S)^2$ where L_S is the width of the neutral plasma region, and $D(x,1) = (Q_{x,z}n_S)^{-1}v(x)_r/3$ with $Q_{x,z}$ equal to the Langevin plus hard-sphere cross sections. However, residual fields that accelerate the thermal cations toward the sheaths normally exist within the quasineutral plasma region, and the actual $R(x,1)_D$ will normally exceed this value. The size of this effect is not known, but the same field acts on all cations and mobilities are proportional to diffusion coefficients, so we will account for it by multiplying $R(x,1)_D$ by a single factor D_p. Electron collisions with silane produce cations at a considerably greater rate than anions, so most cations are lost by diffusion. (An exception occurs at very high P, L, and G, where electron attachment to radicals is important.) Thus, we adjust the factor D_p to yield charge neutrality; in practice D_p is usually 1–5. Summarizing,

$$R(x,1)_D = D_p v_r[3n_S(Q_{\text{HS}}+Q_L)]^{-1}(\pi/L_S)^2 \tag{B10}$$

is used, where the hard-sphere cross section Q_{HS} and Q_L are given (as rate coefficients) in Eqs. (B7) and (B8a) and $L_S = 0.6L$ will be used. Note that $R(x,1)_D \propto x^{-0.5}$ for the small-x values that contribute most of the positive ion loss. These diffusion rates are shown for $D_p = 1$ and typical conditions in Fig. 2.

APPENDIX C: MULTIPLE CHARGING OF PARTICLES

$V(r)$ outside the particle in Fig. 3 is the Coulomb potential felt by one electron when a second is centered within the particle. When the second electron penetrates the particle at $r=r_p$ the electron affinity A_E is subtracted and $V_{\text{in}} = V(r_p) - A_E(r_p)$. We take $A_E(r_p)$ for Si particles from Fukuzawa *et al.* [30], whose result can be represented as $A_E = (4.05-2.9x^{-1/3})$ eV. In the $x=50-1000$ region of primary interest here this yields $A_E = 3.3-3.8$ eV. As indicated in the figure, V_{in} is assumed constant within the particle and the extra Coulomb-repulsion energy is evaluated as $(e^2/4\pi\varepsilon r_{12})$ averaged over uncorrelated electrons uniformly distributed within the particle. The electron kinetic energy associated with confinement is neglected as relatively unimportant. Generalizing to z total electrons, $V(r)_{\text{out}} = (z-1)q^2/4\pi\varepsilon_0 r = E_0(z-1)(1\,\text{nm}/r)$ with $E_0 = 1.44$ eV. In calculating the Coulomb repulsion energy (δ_z) we initially assume that the dielectric constant is that of bulk *a*-Si:H, for which $\varepsilon = 12\varepsilon_0$ similar to crystal Si. We then obtain $\delta_z = 0.12z(z-1)(1\,\text{nm}/R_p)$ eV for z uniformly distributed electrons within the particle.

As can be seen in Fig. 3, if $V_{\text{in}} + \delta_z < 0$ the electrons inside the particle are stable against tunneling out. A calculation shows that if $V_{\text{in}} + \delta_z > 0$ tunneling will occur in a very short time compared to particle-growth rates, so the criteria for stable charging to z electrons is $V(r_p) - A_E(r_p) + \delta_z(r_p) < 0$. This requires $r_p/1\,\text{nm} > 0.35(z-1) + 0.028z(z-1) + 0.12$, where $x = 209(r_p/1\,\text{nm})^3$, which yields $x_2 = 30$, $x_3 = 200$, $x_4 = 720$, $x_5 = 1900$ ($r_{p2} = 0.53$ nm, $r_{p3} = 1.0$ nm, $r_{p4} = 1.5$ nm, $r_{p5} = 2.1$ nm) for the critical x and radius of the first few multiple charges, where the subscript is z. However, $\varepsilon \approx 6\varepsilon_0$ is more appropriate for the crystal Si, $z=2$ case of only 30 Si atoms [31], and an even smaller ε may apply to *a*-Si:H so we will instead use $x_2 = 60$, $r_{p2} = 0.66$ nm for the double-charge limit. It can be seen in Figs. 5–7 that a relatively small fraction of multiply charged particles occur for x values near the limiting values. As a result, the calculation is not very sensitive to this exact size. However, these are much smaller limits than are common in the aerosol field, where water droplets have weaker intermolecular binding and a smaller ε. They are also much smaller than suggested for these Si particles in Ref. [32].

APPENDIX D: INTEGRAL EQUATIONS FOR LARGE-X PARTICLES

The charge ratios $f(x)_z = n(x,z)/n(x,0)$ are obtained by ignoring the x changes associated with the charge-transfer processes in Fig. 4, yielding

$$dn(x,+1)/dt = R(x,0)_{\mathrm{IA}} n(x,0)[R(x,+1)_D + R(x,+1)_{\mathrm{EA}}]n(x,+1),$$

$$dn(x,0)/dt = R(x,-1)_{\mathrm{IA}} n(x,-1) + R(x,+1)_{\mathrm{EA}} n(x,+1) - [R(x,0)_D + R(x,0)_{EA} + R(x,0)_{\mathrm{IA}}]n(x,0),$$

$$dn(x,-1)/dt = R(x,-2)_{\mathrm{IA}} n(x,2) + R(x,0)_{\mathrm{EA}} n(x,0) - [R(x,-1)_{\mathrm{EA}} + R(x,-1)_{\mathrm{IA}}] \times n(x,-1), \text{ etc.} \quad \text{(D1)}$$

For steady state the left side of equations (D1) are 0, and particle growth and loss is then calculated using a $x \rightarrow x+1$ transfer rate $\mathrm{Tr}(x)$ and diffusive loss rate $L(x)$,

$$dF(x)/dx = -[1 + \mathrm{Tr}(x)/L(x)]^{-1} F(x), \quad \text{(D2)}$$

where

$$\mathrm{Tr}(x) = n(x,0) \sum_z f(x)_z [R(x,z)_R + R(x,z)_S + R(x,z)_{\mathrm{IA}}],$$

$$L(x) = n(x,0)[R(x,0)_D + R(x,+1)_{\mathrm{IA}}/f(x)_{+1}].$$

Here $F(x) = n(x)_{\mathrm{tot}}\,\mathrm{Tr}(x)$ is the $x \rightarrow x+1$ flux and $n(x)_{\mathrm{tot}} = \Sigma n(x,z)$ summed over z. The approximations in Eqs. (D1) and (D2) are appropriate at large x, where comparing results to the iterative solution yields excellent agreement for $x > 10^4$. Agreement is also obtained for $10^2 > x > 10^3$ if a minor correction is applied to the $f(x)_z$ ratios to allow for the finite x range over which each anion (of charge $-z$) reaches a steady-state ratio after it initially appears.

APPENDIX E: PARTICLE-GROWTH EQUATIONS FOR $X < 200$

For $x < 200$, the ''particle'' with x Si atoms and the radical or ion with y Si atoms are frequently indistinguishable. For $x < 30$ each neutral radical x' is formed by radical-radical reactions and by cation-anion neutralization, in each case with $x + y = x'$. (Recall that cation-electron neutralization is small and ignored.) The x' radical is lost by reaction with all other radicals, by electron attachment and by diffusion to the electrodes. (Anion and cation attachment yield very minor loss rates, and are ignored here.) Thus, for $x = 1-60$, each iteration uses

$$n(x,0) = \left\{ \sum_{y=1}^{x-1} k(y,x-y)_{\mathrm{RR}} n(y,0) n(x-y,0)/2 + R(x-1)_{\mathrm{IA}} n(x-1,-1) + R(m)_{\mathrm{EA}} n(x,1) \right\} L_O(x)^{-1}, \quad \text{(E1)}$$

where the loss rate is

$$L_0(x) = \sum_{y=1}^{30} k(y,x)_{\mathrm{RR}} n(y,0) + R(x)_{\mathrm{EA}} n_e + R(x,0)_D.$$

The cation x' similarly results from radical-cation collisions with $x + y = x'$ assumed, plus silane collision with the $x-1$ cation. It is lost, with rate $L_1(x')$, by electron attachment, silane collision, diffusion to the sheath, collisional neutralization with all anions, and growth by collision with all radicals. Thus, each iteration uses

$$n(x,1) = \sum_{y=1}^{x-1} k(x-y,y)_{\mathrm{IR}} n(x-y,0) n(y,1) + R(x-1,1)_S n(x-1,1) L_1(x)^{-1}, \quad \text{(E2)}$$

with

$$L_1(x) = R(x,1)_{\mathrm{EA}} + R(x,1)_D + R(x,1)_S + \sum_{y=1}^{30} k(y,x)_{\mathrm{IR}} n(y,0) + \sum_{y=1}^{200} k(y,x)_{\mathrm{II}} n(y,-1).$$

The anion growth equation for each iteration is

$$n(x,-1) = \sum_{y=1}^{x-1} k(x-y,y)_{\mathrm{AR}} n(y,0) n(x-y,-1) + R(x-1,-1) + R(x,0)_{\mathrm{EA}} L_{A1}(x)^{-1}, \quad \text{(E3)}$$

where the loss rate is

$$L_{A1}(x) = R(x,-1)_S + \sum_{y=1}^{30} k(y,x)_{\mathrm{AR}} n(y,0) + \sum_{y=1}^{100} k(y,x)_{\mathrm{II}} n(y,1).$$

Iteratively solving Eqs. (E1)–(E3) for each step of $x = 2-60$ requires already knowing $n(y,0)$ for $y = 1-30$, $n(y,1)$ for $y = 1-100$, and $n(y,-1)$ for $y = 1-200$. This quandary is solved by assuming an analytic form for each $n(y,z)$, using this to evaluate the sums in $L_0(x)$, $L_1(x)$, and $L_{A1}(x)$, iteratively solving Eqs. (E1)–(E3) for $x = 2-60$, and comparing the resulting $n(x)_z$ to the assumed values. The parameters in the analytic forms are then improved and the iteration is repeated until the solution closely resemble the assumed $n(x,z)$. This procedure is much easier than it sounds, first because the $n(x,0)$ for $x = 1-30$ are almost entirely determined by radical-radical reactions and radical diffusion [Eq. (E1) with $R(m)_{\mathrm{EA}} = R(x-1)_{1\mathrm{A}} = 0$]. The approximation $n(x,0) = n(1,0)x^{-B}$ yields an excellent fit to the full solution for $x = 1-10$, which covers the significant radicals. Normally $B = 2-4$, with a larger value corresponding to smaller G, P, or L. Next, the rapid anion-silane reaction leads to a nearly constant $n(x,-1)$ for $x = 1-100$, followed by a rapid decrease for larger x. Thus, for the purpose of calculating the anion sum in $L_1(x)$, it is sufficient to assume $n(x,-1) = n_-/100$ for $x = 1-100$, and $n(x>100,-1) = 0$, where n_- is the total anion charge. This approximation leads

to rapid convergence because $k(y,x)_{\mathrm{II}}$ varies quite slowly with y [see $k(1,x)_{\mathrm{II}}$ in Fig. 1]. Finally, the cation-silane reaction leads to a major peak in $n(x,1)$ near $x=6$ (Fig. 5), and $k(x,y)_{\mathrm{II}}$ varies slowly with y, so assuming $n(x,1) = n_+ \delta(y-6)$ yields a very good initial approximation to the sum in $L_{A1}(x)$, where n_+ is the total cation charge.

For $x>60$, carrying out any of the sums in Eqs. (E1)–(E3) is cumbersome, time consuming, and unnecessary since they are slowly varying functions of x. So for $x>60$ we also replace the (source) sums in the numerators of Eqs. (E1)–(E3) with approximations. Since radicals yield the most particle growth, the most important approximations are

$$\sum_{y=1}^{x-1} k(y,x-y)_{\mathrm{RR}} n(y,0) n(x-y,0)/2 = k(1,x-1)_{\mathrm{RR}} n(1,0) M_R , \tag{E4}$$

and

$$\sum_{y=1}^{m-1} k(x-y,y)_{\mathrm{II}} n(x-y,0) n(y,1) = k(1,x-1)_{\mathrm{IR}} n(1,0) M_1 n(x-1,1) + k(x-6,6)_{\mathrm{IR}} n(x-6,0) n_+ . \tag{E5}$$

In Eq. (E4), the use of a constant multiplier M_R, independent of x, is valid for large x. It typically underestimates the exact multiplier by ~1% by $x=100$, but this has a negligible consequence if the same factor is used in both the numerator and denominator $[L_0(x)]$ of Eq. (E4). This also applies to the constant multiplier M_1 of Eq. (E5), which represents the light radical part of the cation growth, and loss in $L_1(x)$. The remaining term in the approximation of Eq. (E5) comes from the light ions.

[1] J. E. Daugherty, R. K. Perteous, M. D. Kilgore, and D. B. Graves, J. Appl. Phys. **72**, 3934 (1992).

[2] D. M. Tanenbaum, A. L. Laracuente, and A. Gallagher, Appl. Phys. Lett. **68**, 1705 (1996); L. Boufendi, A. Plain, J. Ph. Blondeau, A. Bouchoule, C. Laure, and T. Toogood, Appl. Phys. Lett. **60**, 169 (1992).

[3] M. A. Childs and A. Gallagher, J. Appl. Phys. **87**, 1076 (2000). The reported film growth rate G should be increased by a factor of 4/2.6=1.54. Film growth was measured with interference fringes; each represents a thickness increase of $\lambda/2\ n$, where n is the film index of refraction. This correction results from reducing n to 2.6 from the originally assumed value of 4.0. The 4.0 value is typical for films deposited at 240 C, whereas we recently measured 2.6 for films deposited at 22 C, as in Ref. [3].

[4] U. I. Schmidt, B. Schroder, and H. Oechsner, Thin Solid Films **233**, 297 (1993).

[5] R. M. Roth, K. G. Spears, G. D. Stein, and G. Wong, Appl. Phys. Lett. **46**, 253 (1985).

[6] G. Selwyn, J. E. Heidenreich, and K. L. Haller, J. Vac. Sci. Technol. A **9**, 2817 (1991).

[7] R. N. Carlile, S. Geha, J. F. O'Hanlon, and J. C. Stewart, Appl. Phys. Lett. **59**, 1167 (1991).

[8] B. M. Jelenkovic and A. Gallagher, J. Appl. Phys. **82**, 1546 (1997).

[9] C. Bohm and J. Perrin, J. Phys. D **24**, 865 (1991).

[10] S. J. Choi and M. J. Kushner, J. Appl. Phys. **74**, 853 (1993).

[11] J. Perrin, O. Leroy, and M. C. Bordage, Contrib. Plasma Phys. **36**, 1 (1996).

[12] J. R. Doyle, D. A. Doughty, and A. Gallagher, J. Appl. Phys. **68**, 4375 (1990).

[13] N. I. Itabashi, N. Nishiwaki, M. Magane, T. Goto, A. Matsuda, C. Yamada, and E. Hirota, Jpn. J. Appl. Phys., Part 1 **29**, 585 (1990).

[14] Wm. C. Hinds, *Aerosol Technology* (Wiley, New York, 1982).

[15] Ch. Hollenstein, J.-L. Dorier, J. Dutta, L. Sansonnens, and A. A. Howling, Plasma Sources Sci. Technol. **3**, 278 (1994).

[16] M. Shiratani, H. Kawasaki, T. Fukuzawa, H. Tsuruoka, T. Yoshioka, and Y. Watanabe, Appl. Phys. Lett. **65**, 1900 (1994).

[17] W. M. M. Kessels, M. C. M. van De Sanden, and D. C. Schram, Appl. Phys. Lett. **72**, 2397 (1998).

[18] A. Gallagher, in *Particle Growth in Silane rf Discharges*, edited by H. M. Brantz *et al.*, MRS Proceedings Symposia No. 557 (Materials Research Society, Pittsburgh, 1999) pp. 3–12.

[19] L. Boufondi, A. Plian, J. Ph. Blondeau, A. Bouchoule, C. Laure, and M. Toogood, Appl. Phys. Lett. **60**, 169 (1992).

[20] U. Kortshagen and U. Bhandarkar, Phys. Rev. E **60**, 887 (1999).

[21] A. Matsuda, K. Nomoto, Y. Takeuchi, A. Suzuki, A. Yuuki, and J. Perrin, Surf. Sci. **227**, 50 (1990).

[22] A. Nurrudin, J. R. Doyle, J. R. Abelson, J. Appl. Phys. **76**, 3123 (1994).

[23] M. J. Kushner, J. Appl. Phys. **63**, 2532 (1988).

[24] R. Winkler, M. Capitelli, C. Gorse, and J. Wilhelm, Plasma Chem. Plasma Process. **10**, 419 (1990).

[25] A. P. Hickman, J. Chem. Phys. **70**, 4872 (1979).

[26] M. T. Cuberes, A. Bauer, H. J. Wen, V. M. Prietsch, and G. Kandl, J. Vac. Sci. Technol. B **12**, 2422 (1994).

[27] P. Chantry, A. V. Phelps and G. D. Schulz, Phys. Rev. **152**, 81 (1966).

[28] Ch. Hollenstein, W. Schwarzenbach, A. A. Howling, C. Courteille, J.-L. Dorier, and L. Sansonnens, J. Vac. Sci. Technol. A **14**, 535 (1996); A. A. Howling, L. Sansonnens, J.-L. Dorier, and Ch. Hollenstein, J. Appl. Phys. **75**, 1340 (1994).

[29] J. Doyle, R. Robertson, G. H. Lin, M. Z. He, and A. Gallagher, J. Appl. Phys. **64**, 3215 (1988).

[30] T. Fukuzawa, K. Obata, H. Kawasaki, T. Yoshioka, M. Shiratani, and Y. Watanabe, J. Appl. Phys. **80**, 3202 (1996).

[31] Lin-Wang Wang and A. Zunger, Phys. Rev. Lett. **73**, 1039 (1994).

[32] T. Fukuzawa, M. Shiratani, and Y. Yatanabe, Appl. Phys. Lett. **64**, 3098 (1994).